EJSIT
European Journal of Science, Innovation and Technology
ISSN: 2786-4936
www.ejsit-journal.com
Volume 3 | Number 5 | 2023

On Sea Level Variability, Climate Factors, Trends and Attribution

Dr. Leonard J. Pietrafesa[1,2*], Dr. Shaowu Bao[1], Dr. Satish Kumar[3], Dr. Paul T. Gayes[1], Dr. Thomas Karl[1], Dr. Hongyuan Zhang[1], Ms. Tasnia Rahman[3], Ms. Juliana Kowal[1]
[1]School of Coastal & Marine System Science,
Coastal Carolina University,
P.O. Box 261954, Conway, South Carolina 28528, United States
[2]College of Sciences, North Carolina State University,
Raleigh, North Carolina, United States
[3]Department of Cleveland State University,
Cleveland, Ohio, United States

ABSTRACT

Property, commerce and ecosystem assets across the planet are located at or near the coast, thus are vulnerable to sea level variability and rise. Sea level variability along the boundaries of the ocean basins are critical. We consider eleven relatively long continuous coastal water level time series from open ocean coastal stations around the globe, along with the satellite altimeter time series. The sea level time series are analyzed for internal frequency and amplitude modulated modes of variability and overall trends. Additionally, climate factors related to oceanic and atmospheric heat purveyors and reservoirs are analyzed in-kind. The results confirm that oceanic and atmospheric temperature variability and the disposition of heat accumulation, display complimentary internal modes of temporal variability to those of sea level variability on monthly to annual to inter-annual to decadal and multi-decadal time scales. For future prognostications of coastal and inland inundations of oceanic waters, and for the interactive coupling of coastal to inshore water systems and compound flooding, the coastal-downstream boundary conditions must be prognosticated based upon climate and weather relationships. This is an effort to reveal those relationships. Finally a causal relationship between sea level rises globally to fossil fuel burning, is established within.

Key words: tide gages, ocean temperatures, climate factors, sea level variability, sea level rise, trends, fossil fuel burning, attribution

INTRODUCTION

Sea Level Rise (SLR) is generally considered a slowly evolving global pandemic taking decades to materialize. However, so-called King Tide or Blue Sky flooding has now become a global phenomenon and is showing up routinely several times per year in coastal cities (Figure 1) as originally predicted by Pietrafesa (2000). Coastal water level data generally consists of the deterministic astronomical tides and a rich, robust spectrum of signals representing non-stationary and non-linear processes including variability in local or regional wind fields, precipitation, land runoff, land uplift, the practice of draining coastal aquifers, coastal sedimentation and a host of other conditions. As such, local communities attempting to mitigate growing impacts from changing sea level are constrained by difficulties in trying to apply global scale sea level predictions to communities experiencing complex trends. An additional difficulty stems from traditional data analysis techniques challenged in revealing the information that buried within the time series of coastal tide gauge data. Moreover, attempting to compute numbers defining SLR or the lack thereof, i.e. trends, is not a straightforward process with even the word trend, per se, historically poorly defined and understood.

* Corresponding Author

Sea level is the height of the surface of the open ocean surface relative to a datum or zero reference point. The vertical datum is a collection of specific points on the Earth with known heights either above or below mean sea level. Near coastal areas, mean sea level is determined with a tide gauge. In areas far away from the shore, mean sea level is determined by the shape of the geoid. Similar to the survey markers used to identify known positions in the horizontal datum, many positions in the vertical datum are marked by steel rods driven into the ground with a hinged access cover. Using a technique called differential leveling, a known elevation at one location is used to determine the elevation at another location. As with horizontal datum's, the advanced technology of GPS has almost completely replaced this classical technique of vertical measurement. In 1929, the National Geodetic Survey (NGS) compiled all of the existing vertical bench marks and created the National Geodetic Vertical Datum of 1929 (NGVD 29). Since then, movements of the Earth's crust have changed the elevations of many bench marks. In 1988, NGVD 29 was mathematically adjusted to remove inaccuracies and to correct distortions. This datum, called the North American Vertical Datum of 1988 (NAVD 88), is the most commonly used vertical datum in the United States today. In 2022, scientists at the National Geodetic Survey are scheduled to complete 15-year-long project to update the vertical datum, which will make accurate height measurement better, faster, and cheaper. This project is called the Gravity Definition for American Vertical Datum, or GRAV-D for short (https://oceanservice.noaa.gov/education/tutorial_geodesy/geo06_vert.html). When this effort is completed, users will be able to get accurate heights to within about an inch for most locations around the nation. Nonetheless, changes occurring over short time scales, such as seasons to multiple years are not accounted for and this is a serious liability for setting the downstream boundary conditions in numerical modeling of coastal inundation and inland and upland flooding.

Along coastlines, including estuaries, harbors and river systems and lakes, water level has been measured directly using different mechanical measuring systems from the middle 19th Century to the present. Over the past four-decades, satellite altimeters have been measuring sea level globally from space with varying degrees of spatial and temporal resolution as well. The satellite altimeters have not taken the same global tracks and thus variations between sea surface heights measured by the different satellites exist. In addition, the word relative is germane, as the description of the rise and fall of water level at a spatial location is relative to a vertical datum point on the adjacent land. The land itself may be fixed, i.e. not moving, or could be undergoing uplift or subsidence and as such, the apparent rate of rise or fall of the water in the adjacent water body must be assessed against the land movement. This is not a straightforward exercise.

a) b)

Figure 1. King Tide Blue-Sky Nuisance Flooding on the same day in November 2021: a) in downtown Miami FL; and b) in a restaurant in Thailand

Local mean sea level (MSL) expressed through coastal sea level rise and fall, are governed deterministically by the astronomical tides, due principally to the gravitational effects

of the triad, the Moon, Sun and Earth. It is of important note that the astronomical tides are the only deterministic phenomena in the global ocean basins, i.e. in the ocean sciences. The astronomical tides are entirely predictable. However, never do the astronomical tide predictions agree with the amplitude of water levels that actually occur at any locale. The additional components dictating local sea level are based on isostasy, coastal atmospheric winds, oceanic waves, atmospheric pressure, river and estuary interactions with the coastal ocean, ground water sources and local to regional to basin wide oceanic temperatures and heat content. The realization of these components is dictated by the confluence of a myriad of potential processes. These processes include but are not limited to: addition of fresh water due to melting of Alpine glaciers, polar ice sheets and winter snows; auto-compaction of ancient sediments; compaction of deep sediments, particularly in deltaic environments; crustal loading of riverine sediments; variations in regional to local isostatic rebound from the last period of glacial loading; local to regional slumps in coastal areas due to sediment discharge loading; slumping due to drainage of local ground-water (i.e. subsurface fluvial withdrawal); subsidence from sub-surface withdrawal of fossil fuels; precipitation or the lack thereof and coupled watershed responses; steric rises (falls) of the water levels of adjacent ocean basin water masses due to increases (losses) in the heat content of these water masses; mesoscale to synoptic scale to longer period coastal winds; management practices such as dikes and impoundments that can deprive the coast from naturally flowing river waters and or may enhance soil subsidence; the redirecting of river systems; and global warming due to anthropogenic influences. We will discuss the internal modes of variability revealed by the decomposition of the data time series and the apparent correlations with climate factors. All of these components lead to very specific, community level, differences in sea level for coastal locations (Figure 2). However, there is a huge variation in the estimates of the future SLR. It is of note that land subsidence is an important player in relative sea level rise. Some land subsidence, is related to deep natural processes over long periods of time, such as responding to plate tectonic activity or to the retreating of the glaciers from the last Ice Age. Other sinking is linked to human activity, including extracting oil, water or minerals from underground. In cities, buildings can also add weight and push land down. Many of the fastest sinking places in the world appear in populated areas in Southeast Asia largely because of groundwater extraction, but the U.S.A. faces substantial land subsidence. There, you may not notice land settling around you in your daily life, but scientists found that many places are sinking faster than global sea levels are rising, increasing flood risk in coastal cities. As these changes in coastal sea level are manifest in the data from these locales, they are not adjusted as they represent the facts and contribute to the internal modes of variability that are carried within the gage data.

The recent 33rd State of the Climate Report reported that greenhouse gas concentrations, global sea level and ocean heat content reached record highs in 2022. The international annual review of the world's climate, led by scientists from the National Oceanic & Atmospheric Administration (NOAA) National Centers for Environmental Information (NCEI) at https://www.ncei.noaa.gov, and published by the Bulletin of the American Meteorological Society (BAMS of the AMS), is based on contributions from more than 570 scientists in over 60 countries. It provides the most comprehensive update on Earth's climate indicators, notable weather events and other data collected by environmental monitoring stations and instruments located on land, water ice and in space. "This report is a truly international effort to more fully understand climate conditions around the globe and our capacity to observe them," said NCEI Director Derek Arndt. "It is like an annual physical of the Earth system, and it serves present and future generations by documenting and sharing data that indicate increasingly extreme and changing conditions in our warming world. This report claims that oceanic heat and global sea level were the highest on record in 2022. Over the past half-century, the ocean has stored more than 90% of the excess energy trapped in Earth's system by greenhouse gases and other factors.

The global ocean heat content, measured from the ocean's surface to a depth of 2,000 meters, continued to increase and reached new record highs in 2022. Global mean sea level was record high for the 11th-consecutive year, reaching about 101.2 mm (4.0 inches) above the 1993 average when satellite altimetry measurements began. It discusses that SLR is happening for two principal reasons. First, water expands as it warms. Thus, the ocean is heating up globally, that is storing more heat, thus is literally swelling and has nowhere to go but upward and onto adjacent land masses. Second, more water is pouring into the sea as the ice on mountaintops and ice sheets in Greenland and Antarctica keep melting. The report states that by 2100 the increase in sea levels could be as little as another eight inches, or as much as six-feet-seven inches with two intermediate projections. Thus, by the year 2100, 2 billion people or about one-fifth of the world's population projected for 2100, could become climate change refugees due to rising ocean levels (Figure 2). Another NOAA report (Sweet et al., 2022) predicts a SLR along all U.S. oceanic and gulf coastlines of at least a foot by 2050. If either or both estimates come to fruition, those who once lived on coastlines will face displacement and resettlement bottlenecks as they seek habitable places inland. While these reports have received broad media coverage globally, few policy makers are taking stock of the significant barriers blocking that future coastal climate refugees, like other refugees, will encounter when they migrate to higher ground. Still these estimates are at best wide ranging guestimates. Society in general needs better numbers that are tied to climate factors, perhaps correlatively, and perhaps even to fossil fuel burning, causally. Society needs to know if correlations of sea level variability (SLV) and SLR can be linked to climate factors and perhaps causally to anthropogenic influences that is with attribution, in ways that that can be verifiably predicted. Correlations or the lack thereof, is the goal of this study. We note however, the rate of SLR is not a well-posed mathematical variable, but rather relies upon the definition of a trend. Global sea level trend estimates made by NOAA are presented in Figure 3.

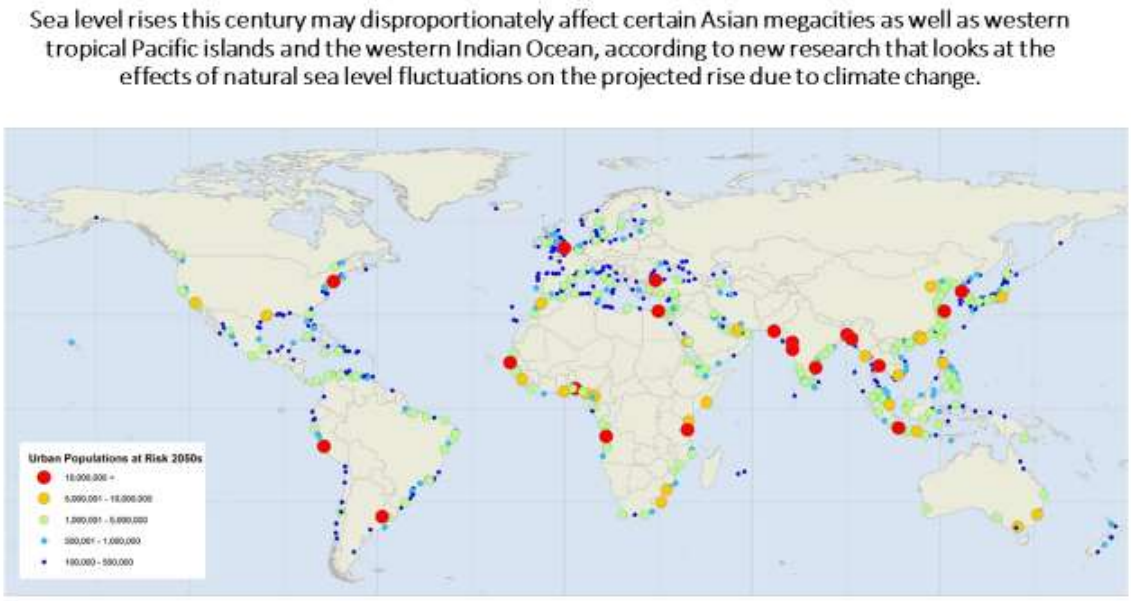

Figure 2. Urban populations at Risk by 2050 due to Sea Level Rise

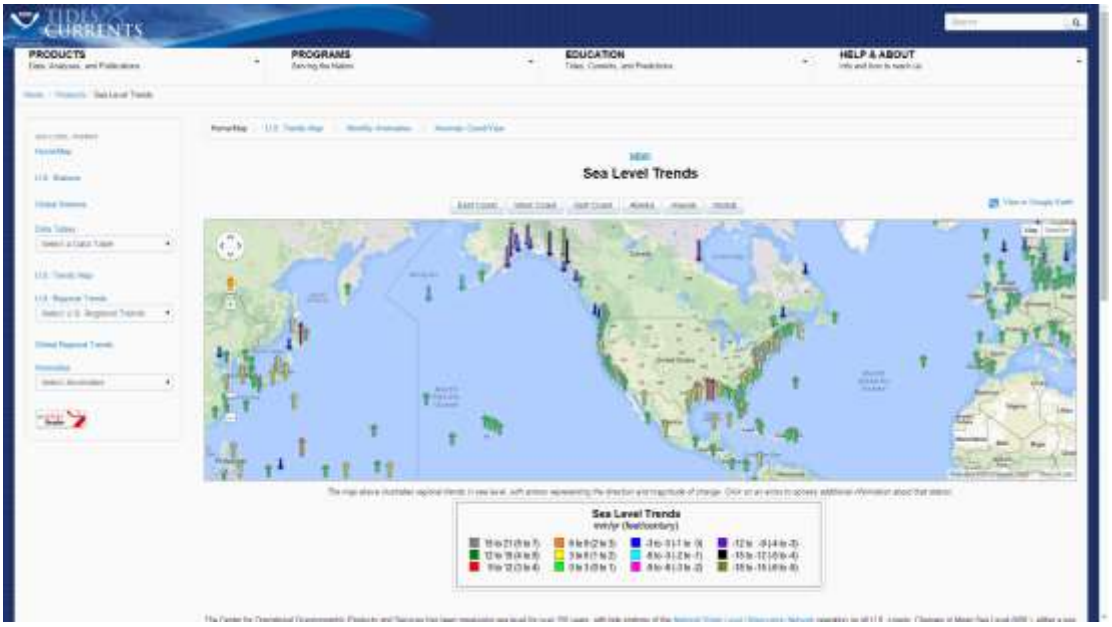

Figure 3. Screenshot of sea level trends from tide gauges around the world from NOAA's sea level rise viewer. Note the widely variable rates of sea level change, both rising and falling (http://tidesandcurrents.noaa.gov/sltrends/sltrends.html), while reported rates of average, global sea level rise are around 3.2 mm/year.

There is some community confusion in assumptions about the computation of SLV and SLR. For example, some believe that if you average hourly coastal water level time series beyond the diurnal period, you simply get tidal residuals; i.e. that all processes beyond diurnal are stochastic and cancel out. Others believe that the two principal contributors to SLV and SLR are oceanic heat storage and polar icecap melting, so the ARGO global drifter network and the GRACE satellite, which separately and respectively measure heat content and land water input to the ocean result in the sum total of SLV and SLR, as depicted in Figure 4. While it is true that satellites, particularly those in the Jason Class, provide global coverage versus the in-situ, site-specific coastal sea level stations (Figure 4, upper left). It is also true that different altimeters have yielded differing results (Figure 4, upper right) and that ARGO has historically only measured ocean heat down to 700m, though more recently some drifters have submerged to depths of 2000m. However, one cannot simply assume that the remainder in SLR estimates is due to melt-waters (Figure 4, lower left). Unfortunately, the ARGO measurement and the GRACE measurements, which should equal the JASON measurements, do not (Figure 4, lower right).

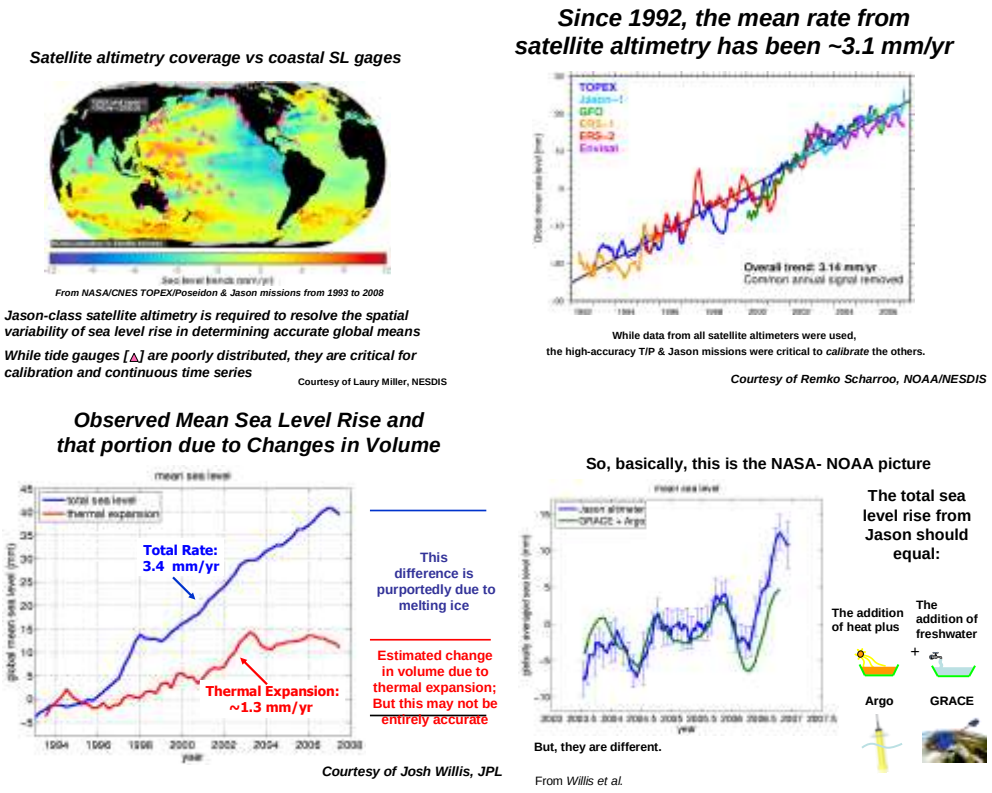

Figure 4. left) Global coverage of satellite altimeters vs In-Situ Gages; middle left) Different satellite altimeter measurements of SL; middle right) the portions of SLR attributed to oceanic heat, measured by ARGO, and melting ice, measured by GRACE, which should equal JASON's observations, and JASON altimeter observations; right) which integrates ARGO plus GRACE. However, as shown, the numbers do not add up.

Across the U.S., responsible state and local officials are now beginning to develop policies that address the anticipated and perceived consequences of climate variability and change. For coastal communities, a significant concern is based on numerous publications which claim significant global accelerations in the rate of SLR. If true, the documentation of acceleration of SLR globally (Church & White, 2006) and or regionally (Salinger et al., 2012; Bromirski et al., 2012) and the resulting erosion and inundation of coastal resources presents a significant societal concern. However, Houston and Dean (2011) claimed that the rates of SLR are actually decelerating everywhere in U.S. coastal waters. We will test the claims of these and other publications, using mathematical methodologies to decompose the non-linear and non-stationary coastal water level time series. In our discussion to follow, isostatic changes in land surface elevation could have been factored into our estimates to provide relative changes. However, that would serve no purpose as we are seeking correlative evidence of relationships between SLV, SLR and SLR trends versus oceanic and atmospheric climate factors, and not the details of isostatic glacial rebound.

DECOMPOSING AND DE-TRENDING ATMOSPHERIC AND OCEANIC CLIMATE FACTOR DATA

Atmospheric and oceanic climate factor data were harvested from the NOAA NCEI. There is a rich library of climate factors that control seasonal to sub-seasonal variability of sea level around the planet. However, as will be seen these time series are characterized by highly non-stationary and nonlinear temporal variability. As such, it is not clear that any conventional

simple averaging process can be utilized to reflect what information is buried in the multiple time series. This underscores the importance of clearly defining a trend. The James & James Mathematical Dictionary (1976) definition of a trend is: "the general drift, tendency or bent of a set of data". Chatfield (1975) defines "trend" as "a long term change in the mean". However, a difficulty with this latter definition is determining what a long term is mathematically. If variations in climatic variables exhibited a 50-year, cycle and if one were to have only 20 years of data, then the 50-year cycle would appear to be a trend. However, if there were 120 years of data then the 50-cycle would go through two cycles and thus be evident. In speaking of a Chatfield trend, we must take into account the number, span of observations available, and then make a subjective assessment as to what constitutes long term. Granger (1966) defines a trend in a data time series as the mean, comprising all frequency components whose wavelength exceeds the length of the observed time series; a mathematically reasonable estimate. Nonetheless, for nonlinear and nonstationary datasets, none of the above definitions is mathematically applicable.

In our opinion, the seminal publication of Wu et al. (2007) put forward a logical definition of "a trend" which is appropriate for any nonstationary and nonlinear time series. Wu et al. stated: "a trend is an intrinsically determined function within the temporal span, of the data, and a function in which there can be at most one extremum within that temporal span of data". Being intrinsic, the method employed to derive a trend has to be adaptive that is, it must suit the span of the data. Thus this definition of trend does make a presumption of the existence of a time scale, related to the span of the data; a logical, mathematically based definition. All the above requirements suggested to Wu et al. (2007) that the Empirical Modal Decomposition (EMD) method (Huang et al., 1998) as the logical choice for an algorithm that could determine the trend in any continuous data set. The 'gravest' intrinsic mode or rather the lengthiest mode of a time series that can be determined by employing the EMD methodology, can go up and or down or down and or up in amplitude, so that there is but one respective maximum or but one respective minimum in this mode. They called this mode the trend of the time series. Once the trend of a time series is determined via using the EMD, the corresponding de-trending operation can be implemented. With this definition of trend, the variability of the data over inherent, intrinsic time scales can be derived. We will employ an advanced form of EMD, the Ensemble EMD (EEMD), as first presented by Wu and Huang (2008), to decompose the data set time series that we will study, and identify all intrinsic modes present in each. What is EMD-EEMD?

The Hilbert Transform (Gabor, 1946) has been applied to calculate the accompanying imaginary part of a time series. It was employed by Huang et al. (1998) to obtain the complex expression of the instantaneous amplitude and frequency in a time series. Due to the Hilbert Transform being a global domain integral, the instantaneous amplitude and instantaneous frequency obtained using the Hilbert Transform is not "temporally local" or instantaneous, the direct quadrature algorithm is implemented to obtain the instantaneous amplitude and instantaneous frequency (Huang et al. 2009).

In the EMD, the data $x(t)$ is decomposed in terms of "intrinsic mode functions" (IMFs), c_j, i.e.,

$$x(t) = \sum_{j=1}^{n} c_j(t) + r_n(t), \tag{1a}$$

where

$$c_j(t) = a_j(t)\cos\left[\int \omega_j(t)dt\right], \tag{1b}$$

and r_n is the residual of the data $x(t)$, after n intrinsic mode functions (IMFs) are extracted from the instantaneous frequency, omega from high frequency to low frequency intrinsic modes

from j=1 to the finite number "j = n", determined via the "sifting" process and which constitute the limits of the integral (i.e. 1 to finite number "j"=n). Here "instantaneous frequency" is defined in context, and the integral can be considered as the local mean for IMF c_n. Clearly, The IMFs expressed in Equation (1b) are simple oscillatory functions with relatively slowly varying and non-negative amplitude and relatively fast changing and non-negative frequency at any temporal point.

In practice, the EMD is implemented through a sifting process that uses only local extrema. From any data set, $x(t)= r_{j-1}$, say, the procedure is as follows: 1) identify all the local extrema (the combination of both maxima and minima) and connect all these local maxima (minima) with a cubic spline as the upper (lower) envelope; 2) obtain the first component *h* by taking the difference between the data and the local mean of the two envelopes; and 3) treat *h* as the data and repeat steps 1 and 2 as many times as is required until the envelopes are symmetric about zero within a certain tolerance. The final *h* is designated as c_j. A complete sifting process stops when the residue, r_n, becomes a monotonic function or a function only containing one internal extremum from which no more IMFs can be extracted. In EEMD, multiple noise realizations, are added to one time series of observations to mimic an ensemble average approach for corresponding IMFs can be used to extract scale-consistent signals.

The major steps of the EEMD method are: 1) add a white noise time series to the targeted data; 2) decompose the data with added white noise into IMFs; 3) repeat step 1 and step 2 again and again, but with different white noise series each time; and 4) obtain the (ensemble) means of corresponding IMFs of the decompositions as the final result. After a time series is decomposed into IMFs, natural amplitude-frequency modulated oscillatory functions, various methods can be applied to obtain instantaneous frequencies for each IMF that lead to time-frequency-amplitude representation of the data.

OPEN OCEAN COASTAL SEA LEVEL DATA AND SATELLITE ALTIMETER DATA

In our study, we selected 11 open ocean water level stations that are globally distributed and long in the overall periods of observations with few disruptions to the hourly time series. Manilla Bay Harbor was seriously disrupted during World War II and we adjusted the missing time series by connecting the end points. All other series are at 99% or greater in being complete. For all of the stations considered, we employed monthly averaged time series thereafter in our EEMD decompositions. Table 1 lists stations, locales and beginning and end dates. The source of these quality controlled coastal, open ocean, water level data is: https://www.star.nesdis.noaa.gov/socd/lsa/SeaLevelRise/LSA_SLR_timeseries.php.

Table 1. 11 Global SL Stations with Start and End Times and SL Values

Station Location	Name (Figure 2)	Start date Mo/Year	Start value Onset-MSL Meters (M)	End Date Mo/Year	End value End-MSL (M) Data Archives	End to End Slopes in cm/yr
Atlantic City, NJ	ACNJ	09/1911	-0.291	10/2021	0.260	0.50014
Galveston, TX	GTX	01/1904	-0.711	10/2021	0.193	0.76721
Honolulu, HI	HONO	01/1905	-0.120	10/2021	0.020	0.11983
Hoek Van Holland	HVH	01/1864	6.344	12/2018	6.988	0.41549
Key West, FL	KWFL	01/1913	-0.179	10/2021	0.089	0.24626
Auckland, Whangarei NZ	AUNZ-BSNZ	11/1903	6.972	12/2018	7.139	0.14511
San Diego, CA	SDCAL	01/1906	-0.176	10/2021	0.059	0.20289
Seattle, WA	SW	01/1899	-0.208	10/2021	0.128	0.27355

Sydney/Ft Denison, Australia	Syd_ftd	01/1886	6.828	12/2018	7.002	0.13084
San Francisco, CA	SFCAL	07/1854	6.91 -0.185	12/2020 03/2023	7.06 0.102	0.09009 0.17000
Manilla Bay Harbor Philippines	MBH	01/1926	6.75	10/2021	7.50	0.78670

The IMFs of the water level time series for Sydney Harbor Australia and San Francisco CA U.S.A. are in Figures 6 a, b. Sydney and San Francisco EEMDs are representative of all other 9 stations. In Table 2, the list of the EEMD IMFs, their modulated periods, the mode amplitudes and the trends are for the 11 coastal water level stations, globally distributed.

For periods shorter than a month, Pietrafesa et al. (2022) demonstrated that subtidal to monthly variability of coastal seal level is determined up to 95% by the along coast component of the wind with an 8-hour lag; so is stochastically deterministic, from hourly out to a month. On an hourly basis, water levels at Charleston not only reflect the astronomical tides but the alongshore component of the wind. If one considers the hourly alongshore components of the winds and water levels at Charleston, then the 60-day plot shown in Figure 5 results. Coastal Frontal, Meso-Alpha to Beta to Gamma to Synoptic scale atmospheric systems of hourly to daily to weekly to several weekly temporal scales are represented in the figure. Basically when the alongshore component of the wind (top panel) blows, with the coast to its left (right) in the Northern Hemisphere (Southern Hemisphere), then water level (middle panel) drops at the coast and when the alongshore component winds blows with the coast to its right (left), in the Northern Hemisphere (Southern Hemisphere), water level rises at the coast, all within an 8-hour lag in the non-tidal response. This is a mechanical response, the coastal spin-up time, on continental shelves (Chao & Pietrafesa, 1980) and carries through from hours to days to weeks to months. Figure 5 bottom panel demonstrates the tight coupling between the alongshore winds and water levels at Charleston. A moving correlation between the two monthly averaged time series over a 62-year period shows that the coupling is very tight. However, taking sea level variability to seasonal to sub seasonal temporal and spatial scales is a leap to be addressed and determined below.

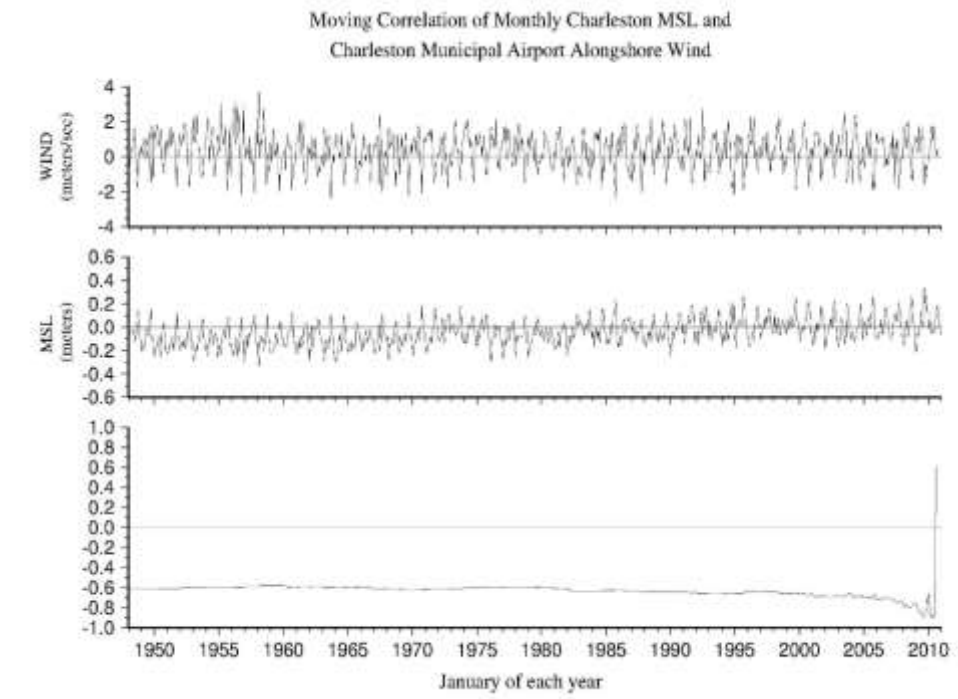

Figure 5. Top panel are hourly along coast winds during 63 years of the months of January with > 0 (<0), winds blow with the coast to their left (right). Middle panel are coastal water levels with the astronomical tides removed. Bottom panel is the cross correlation of the winds and water levels with an 8 hour lag of the latter to the former. This is true for all costal water level stations with the signs reversed in the Southern Hemisphere.

On a daily basis, 24 hourly averaged alongshore winds and coastal water levels with the Semi-Diurnal and Diurnal Tides removed display the following the relationship shown in Figure 6. In the Northern Hemisphere, winds blowing with the coast to their left (right) will drop (raise) sea level at the coast. The opposite occurs in the southern hemisphere. This is a mechanical time dependent coastal Ekman response (Chao & Pietrafesa, 1980).

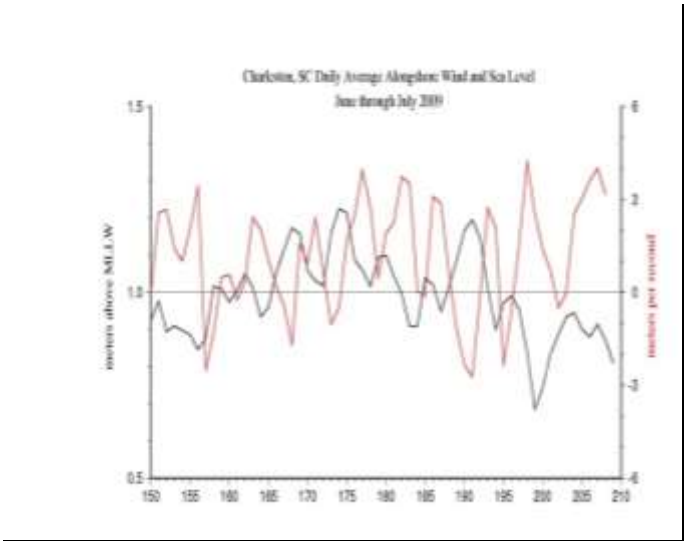

Figure 6. Daily averaged alongshore winds and coastal water levels at Charleston. Wind components positive (the coast to their left) cause water levels to drop. Winds blowing with the coast to their right cause water levels to rise. Time along the horizontal axis is in year-days (Julian). The opposite occurs in the Southern Hemisphere.

As shown in Figures 7 a, b and Table 2, the monthly times series of 2 of the 11 global stations (9 are not shown) can be decomposed into internal modes of variability from IMF1 through IMF 6. The stations with periods in excess of 22 years appear in the Sydney, Auckland, Honolulu, San Diego and San Francisco time series, and not in the other 6. While only two representations of the EEMD decompositions are presented in Figures 6 a, b, the other 9 stations, not shown, are in-kind through Mode 6. The amplitudes of the modes vary from 2 to 15 cm and all modes contribute overall to the resulting time series shown in red in the top panels (representative) in Figures 7 a, b. Table 2 presents modulated periods and modulated peak amplitudes of the internal, intrinsic modes of variability of Sea Level from 11 coastal stations around the Globe and Satellite Altimeters. The Altimeter data time series consists of multiple satellites with global paths and is cleverly blended together but is not regular in time steps, so has an irregular or rather intermittent frequency of observations. Nonetheless, it is useful. The periods of the internal modes of variability (IMFs) for the coastal stations are: 1) = 2-3 months or seasonal; 2) = 5-7 months or winter/fall, spring/summer); 3) = 11-13 months or annual; 4) = 2-3 years or inter-annual; 5) = 4-6 years or multi-year; 6) = 10-12 years or decadal; 7) = 21-23 years or several-decadal; 8) = 44-48 years or multi-decadal. The gravest mode or last IMF of each time series is the overall trend of each of the SL time series.

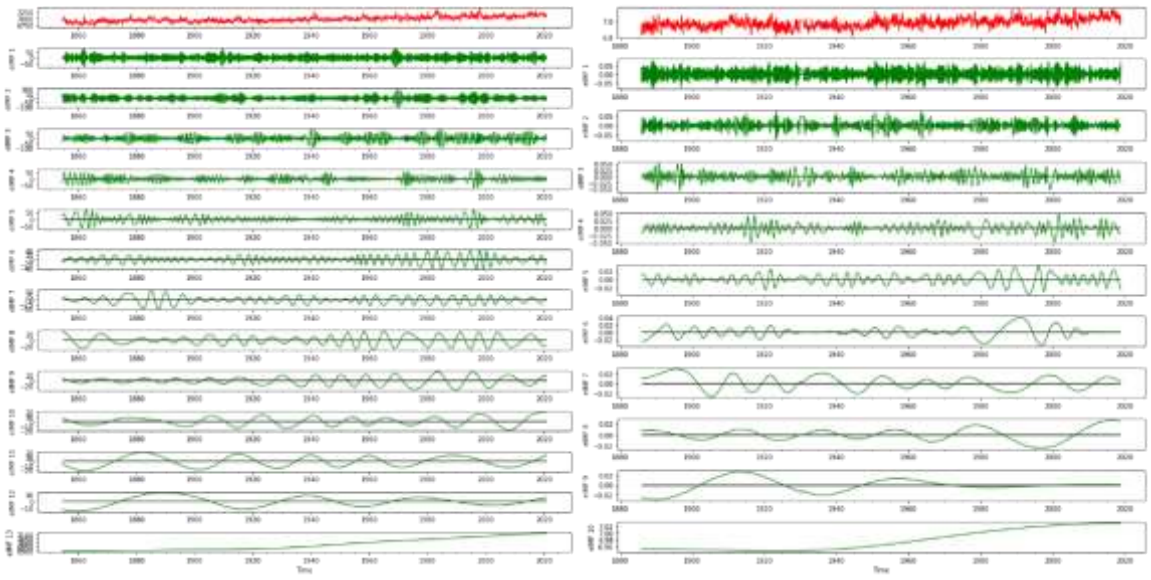

a) b)

Figure 7. EEMD IMFs for: a) San Francisco CA USA (13 Modes); and b) Sydney Australia (10 Modes). Overall water level Trends are IMFs 13 for San Francisco and 10 for Sydney.

We also consider Satellite Altimeter estimates of SLV and SLR. Satellite radar altimeters measure the ocean surface height (sea level) by measuring the time it takes a radar pulse to make a round-trip from the satellite to the sea surface and back. While satellite coverage is relatively short in time, it provides global coverage. That said, many different satellite altimeters have been in the mix and the sensors have not always been uniformly consistent with each other. Nonetheless, the NASA Goddard Center (NGC) and the NOAA National Environmental & Space Data Information Service (NESDIS) ensure quality altimeter data (https://www.star.nesdis.noaa.gov/socd/lsa/SeaLevelRise/LSA_SLR_timeseries_global.php). Satellite Altimeter data (not shown) display considerable spread in observations

up to ~ 2006 when the sensors improved greatly, and thus the spread in the signals was reduced. The satellite time series are referred to as ALT.

It is of note herein that in all of the EEMD decompositions shown above (and the others not shown), the Metonic Cycle does not explicitly appear. The Metonic Cycle or Enneadecaeteris (derived from Greek for "nineteen" years) is a period of 19 years which is remarkable for being a common multiple of the solar year and the synodic (lunar) month. It is of note that globally, 19 years is used as the base period over which a coastal tide gauge station achieves "first order" status. It is over that period that essentially all of the planetary inputs to the Earth's astronomical tidal response are realized and repeated. Thus, if you have 19 years of continuous data, then you have captured all of the astronomical tidal components which will only be repeated over the next 19 year period. This lack of explicit representation would seem to suggest that EEMD has failed. But this is not so, as shown in Figure 8, which consists of hourly data collected from Charleston SC USA over the period 10/1921-04/2007. These time series were employed as there are no beaks in the multi-decadal hourly time series. IMF 2 has an upper and lower bound envelope of 19 years that has a 19-year repeating period. The Metonic Cycle appears as a modulation apparently because it contains all of the deterministic factors of the astronomical tides, as well as the stochastic elements, which contribute to the spikiness and even some aliasing of the record. This finding makes a significant statement about sampling intervals for coastal water level data. If you sub-sample phenomena, which contain both deterministic and stochastic processes, then you will miss key contributors to a time series record. Thus, EEMD has revealed a potential pitfall of sampling theory. To wit, if you sample too infrequently, even when you are attempting to observe a total process that extends from the higher M2 harmonic of 3.1 hours to a full 19 years, the latter of which appears as a modulation of the envelope of IMF 2 (C2 in the figure). Thus, the lesson is that you must capture all of the tide gage components to make the total 19 year record correct. Therefore, for a complete astronomical tidal record, data sampling of no less frequency than one sample per hour, over a period of 19 years in length, is required.

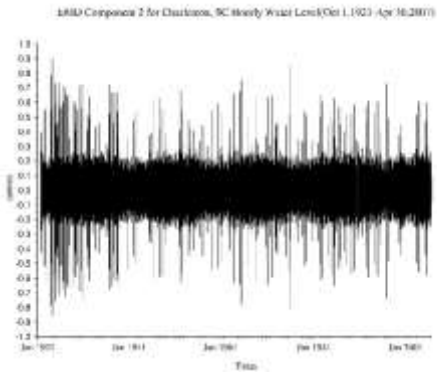

Figure 8. EMD IMF 2 (C2) of the time series of Charleston SC hourly sea level data displays a 19-year modulation of the hourly data. The spikes are high amplitude, short period events in the time series record.

An overview of the internal temporal modes of variability (IMF's) buried within the sea level data are remarkably consistent, centered at 3, 6 and 12 months and 2-3, 5-7 and 11 years for all of the open ocean, coastal stations. All of the stations, except Galveston Bay in the topographically constrained Gulf of Mexico, exhibited a 15 year mode as well. A 22 year mode exists at the 5 stations of Sydney, Seattle, San Francisco, Holland and Key West. An IMF at ~ 33 years shows up in the 3 stations San Francisco, San Diego and Auckland and an ~ 45 year mode appears in the 4 Pacific stations of Honolulu, San Francisco, Auckland and Sydney. The

30-year satellite altimeter time series (ALT), which covers the global ocean, displays IMFs centered at 3, 6, 12 months and 2-3, 5-7 and 11 years, in alignment with all of the 11 coastal stations. In the case of each station, the amplitudes of the IMFs are internally self-consistent, e.g. they are of comparable size relative each to their station specific counterparts. This is especially true of the ALT time series, within which the six IMFs are basically identical in amplitudes of 5 - 6 mm.

Table 1. The Internal Mode Functions (IMFs) and maximum +/- amplitudes in Centimeters of the Monthly Sea Level Time Series of 11 Coastal Water Level Stations

Station Name Country	IMF (#)=> Periods ===➔ Time Series in Years	(1) 2-4 m cms =>	(2) 5-7 m	(3) 11-13 m	(4) 2-3 y	(5) 5-7 y	(6)-(7) 10-12 y	(7) 14-16 y	(8) 21-23 y	(8) - (9) 30-33 y	(8), (9)-(10) 44-48 y	Trend Cm/ Year
Sydney Australia	134 Years	10	10	7	5	4	4	4	3	---	3	0.131
Seattle WA USA	122	13	11	7.5	6	6	5	3	1			0.274
San Diego CA USA	115	4	6	6	5	4	4	4	---	4		0.203
Manilla Harbor Philippines	94	10	10	6	6	6	6	7.5				0.787
Key West FL TX	113	10	10	6	4	4	2	2	2			0.247
Hoek Von Holland	157	15	12	10	10	6	5	3	2			0.416
Honolulu HA USA	116	6	6	7.5	5	6	3	2	---	---	2	0.120
Galveston TX USA	117	11	10	7.5	10	7	4					0.768
Atlantic City NJ USA	118	11	7.5	6	6	4	2.5	2				0.501
San Francisco CA USA	162	2, 3 & 7.5	5-7 & 10	12, 24 & 7.5	7.5	7.5	5	6	3	3	3	0.170
Auckland NZ	117	7	7	6	5	5	5	3	---	3 1st half	3 2nd half	0.146
Satellite Altimeters	30	6 mm 1,3 mn	6 mm	6 m m	6 mm	5 mm	5 mm					0.350

For each of the sea level time series, the last mode or gravest mode is deemed the overall trend of the time series (Wu et al., 2007). The trends of each of the sea level time series are presented in the last column in Table 2 and are plotted in Figures 9a and 9b. In 9a, we display the trends all beginning at zero on the vertical axis. In 9b, each trend has its mean removed and thus they are all normalized relative to zero. All of the sea levels, from our global samples, display significant overall rises, so SL is rising globally. The rates of rise vary significantly as a function of hemisphere and latitude and longitude, with Manilla Bay in the Philippines

displaying a nominally 80 cm rise over 75 years, and Galveston Bay TX displaying an astounding, approximately 90 cm rise over 115 years, each their respective periods of observations. Atlantic City NJ displayed about a half meter rise. We selected stations that were not affected so much by land runoff and river discharge but rather by adjustments in the water levels of the ocean basins that they border. That said, stations such as Galveston TX could well have been victims of land sinking due to human induced freshwater extraction from the groundwater aquifers. Relative rise can be exacerbated by land sinking; but that fact was out of our control as it is impossible to acquire and or confirm. Coastal communities and developers do not generally share that information.

In Figure 10, the rates of rise of the sea level trends (Figures 9a, 9b) are presented. Obviously Manilla Bay and Galveston realized the most rapid rates of rise while Sydney and Auckland displayed the lowest rates of rise. Curiously the rates slowed globally entering the 2nd decade of the 21st Century. These rates may be related to Global Climate Factors. Those will be addressed in the next section. In Table 1 the overall rates of rise of the individual stations are presented. What is remarkable is that satellite altimeters measured an overall global ocean rate of rise of 3.50 cm/year and the rates of rise at the 11 coastal stations collectively averaged 3.43 cm/year. Perhaps, a coincidence, but startling nonetheless. Clearly, as shown by the end points in Figure 9, the rates of rise are not attenuating.

The first derivatives of the trends in sea level rise, presented in Figure 10, display upward and downward oscillations at all stations over periods of decades. However, the 1st derivatives are positive in upward acceleration so while the rates of upward rates of rise in sea levels vary, they are all rising, at differing rates, both individually and from each other.

There does not appear to be biases in total sea level rises or rates of rises as relates to station distributions, either latitudinal or longitudinal.

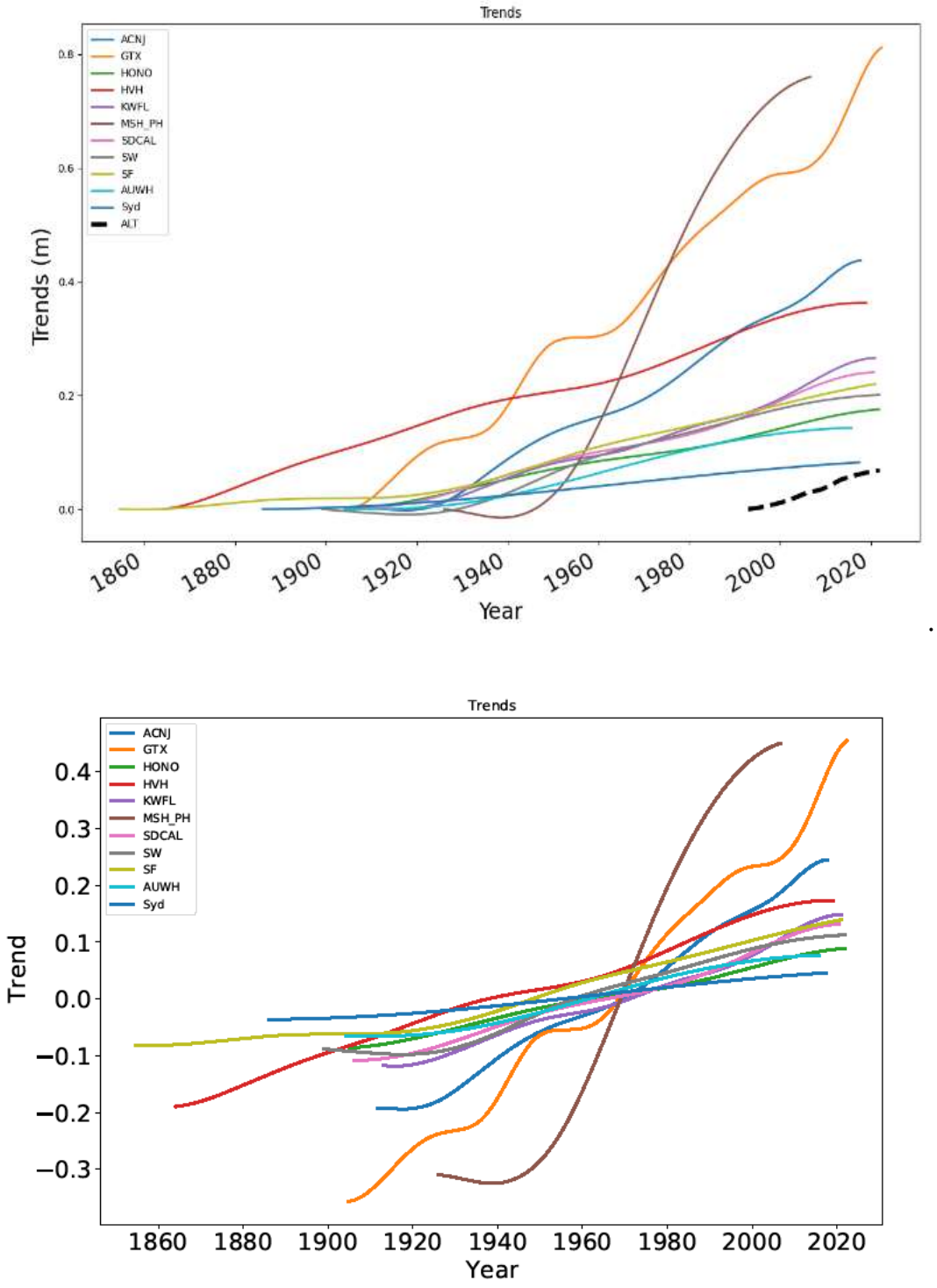

Figure 9. a) Upper Panel: The trends of the 11 coastal sea level time series and altimeters starting at Zero on the vertical axis. The units on the vertical axis are in meters/year relative to Zero. b) Lower Panel: The trends of the 11 coastal sea level time series with their individual record length means removed. The units are in cm/year.

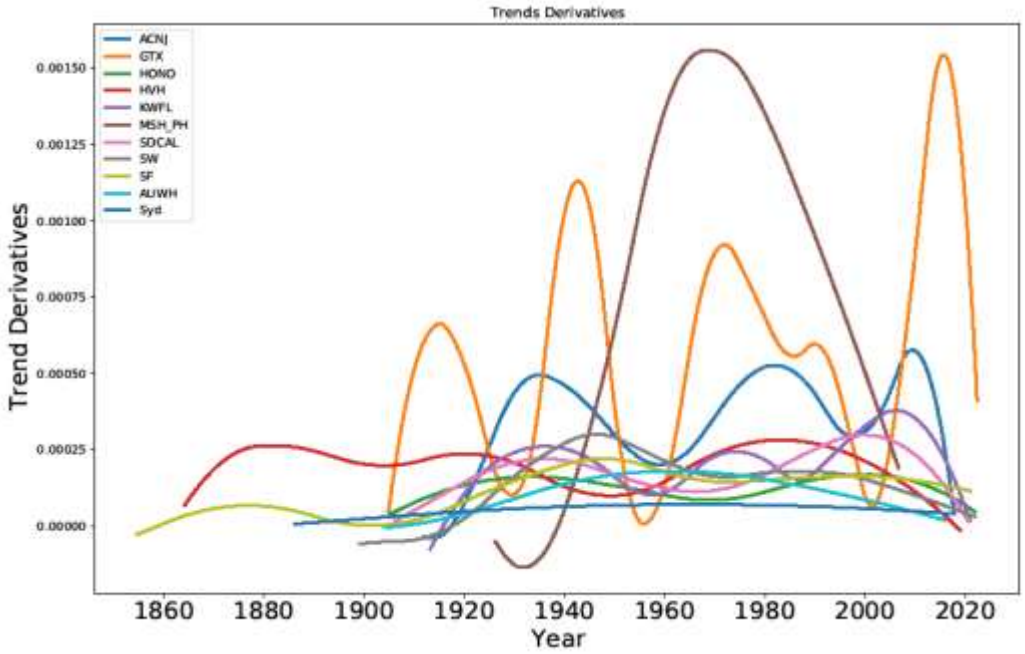

Figure 10. The rates of sea level trend changes over time; i.e. trend first derivatives. Units in the vertical axis are in m/year.

GLOBAL CLIMATE FACTORS

We now look at a number of Climate Factors that SLV and SLR may be associated with and to which there could be visually correlative relationships. To do so, we begin with a discussion of solar variability over time. Arguably, solar activity is the big dog controlling the climate of the Earth. The Sunspot Number is a crucial tool in the study of climate change. In fact, the Solar Sunspot time series is the longest continuous time series of any natural phenomena. However, there have been issues related to Sunspot records over the long period of human observations employing a sequence of varying tools. We now address those given the collective record of Sunspot activity, a significant human undertaking.

The Maunder Minimum, 1645 to 1715, when sunspots were reportedly scarce and winters were documented in the historic record to have been harsh, and thus suggested a link between solar activity and climate change. From 1715 to the present, some 307 years, there is general consensus that solar activity has been trending upwards, reaching a relative peak in the late 20th Century, called the Modern Grand Maximum. This trend has led some scientists to conclude that the Sun has played a significant role in modern climate change. The Wolf Sunspot Time Series is the oldest time series in solar terrestrial physics still in use today, having remained untouched for over 160 years. Established by Rudolf Wolf in 1856, the method is based on both the number of groups of sunspots and the total number of spots within all the groups. In 1994, the question began to arise as to whether the WSN was the correct method of constructing a historical sunspot record. The limitations of early telescopes meant that it was easy for smaller spots to be missed. With this in mind, a new index was established in 1998: the Group Sunspot Number (GSN), which is easier to measure and goes all the way back to the measurements done by Galileo. This index was based solely on the number of sunspot groups. Establishing this system performed a valuable service by finding and digitizing many sunspot observations not known or used by Wolf and his successors, effectively doubling the amount of data available before Wolf's tabulations. Unfortunately, the two series disagreed seriously before about 1885, and the GSN has not been maintained since the 1998 publication of the series. The GSN also revealed a pattern of continually rising solar activity, beginning in the 18th century

and culminating in a Modern Grand Maximum in the latter part of the 20th century, which Wolf's method does not suggest.

However, a discrepancy between two parallel series of sunspot number counts has been a contentious issue among scientists. The two methods of counting the sunspot number, the Wolf Sunspot Number and the Group Sunspot Number 2, indicated significantly different levels of solar activity before about 1885 and also around 1945. With these discrepancies now eliminated, there is no longer any substantial difference between the two historical records. The new correction of the sunspot number, called the Sunspot Number Version 2.0, led by Frédéric Clette (Director of the World Data Centre [WDC]–SILSO), Ed Cliver (National Solar Observatory) and Leif Svalgaard (Stanford University, California, USA), nullifies the claim that there has been a Modern Grand Maximum. It has now been recalibrated and shows a consistent history of solar activity over the past few centuries. The new record has no significant long-term upward trend in solar activity since 1700, as was previously indicated. This suggests that rising global temperatures since the industrial revolution cannot be attributed to increased solar activity. The new results make it difficult to explain the observed changes in the climate that started in the 18th century and extended through the industrial revolution to the 20th Century as being significantly influenced by natural solar trends.

The Sunspot Number is the only direct record of the evolution of the solar cycle over multiple centuries and is the longest scientific experiment still ongoing. The apparent upward trend of solar activity between the 18th century and the late 20th century has now been identified as a major calibration error in the Group Sunspot Number. Now that this error has been corrected, solar activity appears to have remained relatively stable since the 1700's. The newly corrected sunspot numbers now provide a homogenous record of solar activity dating back some 400 years. Figures 11 a, b present the Sunspot time series. Relative peaks in the time series occurred in June 1778 and in March 1858 when 309 and 285, respectively, were recorded.

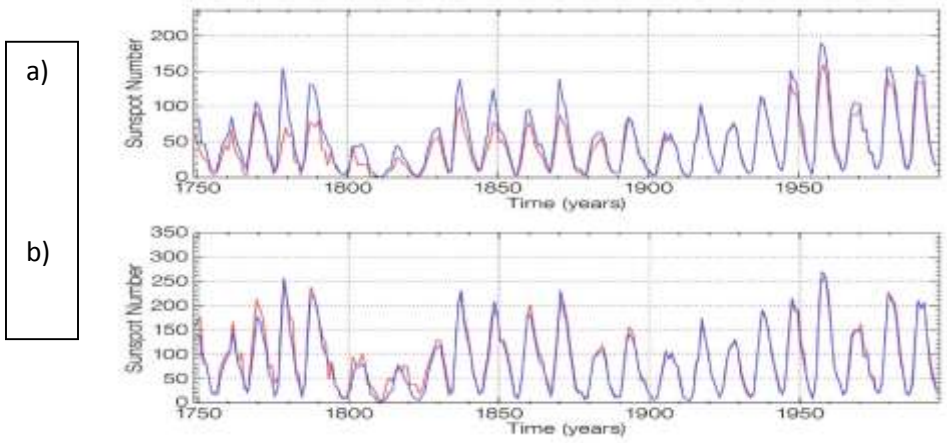

Figure 11. a) The Wolf Sunspot Number versus the Group Sunspot Number (Red Line), which has been adjusted in (b), showing the agreement between the two time series.

In Figure 12, we present the EEMD decomposition of the corrected Solar Sunspot time series (Figure 7 b). Ten internal IMF modes of variability, including the first half of a long cycle (IMF 10), are displayed. The IMF modes are (1) 2-4 months, (2) 5-7 months, (3) 11-13 months, (4) 2-4 years, (5) 10-12 years, (6) 20-22 years, (7) 30-33 years, (8) 110 years, (9) about 150 years, and (10) the first half of a ~ 540 year cycle, rising from 84 to 88 events per year over the 273-year length of the record, and about to begin dropping. We note that IMF 5, the 10-12 year cycle, has the largest amplitude being more than twice those of all other IMF modes, which are all significant in amplitude relative to each other. IMF modes 1, 2, 3, 4 are

all enhanced during high activity years of Mode 5, the nominal mode of reverse polarity of the Sun's magnetic field which occurs over a period centered about 22 years. Because nearly all manifestations are insensitive to polarity, the 11-year solar cycle remains the focus of Solar research; however, the two halves of the 22-year cycle are typically not identical, such that the 11-year cycles usually alternate between higher and lower sums of Wolf's sunspot numbers (the Gnevyshev-Ohl rule). The ~ 44-year cycle may be a lower harmonic of the 11-year magnetic field reversal and the 22-year full reversal period.

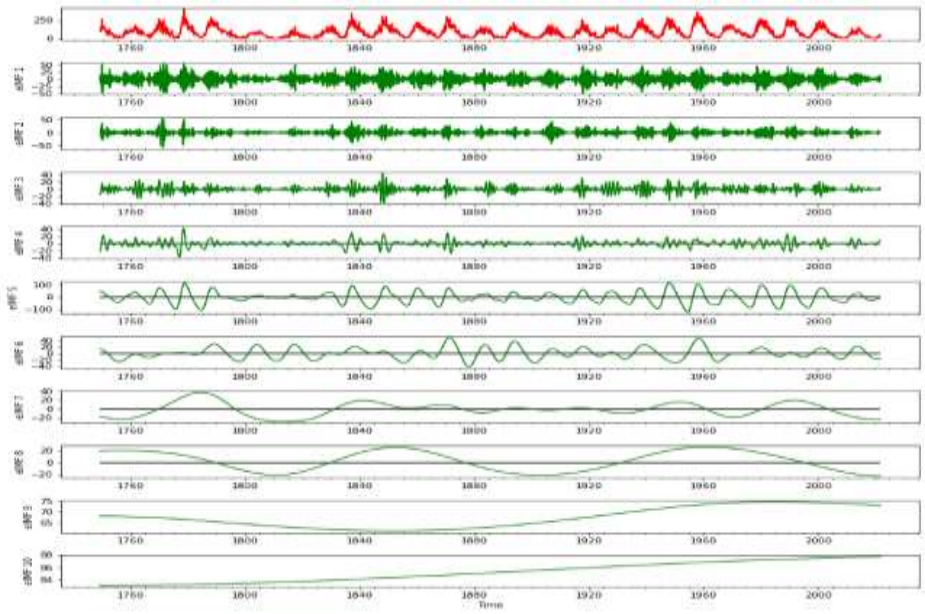

Figure 12. The EEMD Decomposition of the Solar Sunspot Monthly time series presented in the Top Panel (the Red time series). There are eleven internal or IMF modes of variability, including the overall Trend.

In order to investigate the possible relationships between the variability and overall trends in sea levels, we next consider a group of "climate factors", that is, large temporal scale atmospheric and oceanic state variable distributions that may influence SLV and SLR, locally and globally. We will consider them in alphabetical order. Some have lengthy time series and some do not. It should be noted that some of these time series have been "de-trended" and as such may be able to provide attributable relationships to SLV but not to SLR. This averaging should not have been allowed. The raw data should always be quality assessed but not altered. The state variable characteristics of the selected Climate Factors are presented in Table 2. The IMF frequencies and amplitudes are presented in Table 3.

The Quasi-Biennial Oscillation (QBO) is an oscillation of the equatorial zonal wind between easterlies and westerlies in the tropical stratosphere with a mean period of 28 to 29 months. As shown in the QBO panel, Table 2, while the QBO has 9 IMFs, only IMF 4 is significant at 2.2 months and the Trend is flat, perhaps an indication that the men has been removed within the data archive. No climate factor data should be record length averaged. This is a travesty if it was done.

The Atlantic Meridional Mode (AMM) is viewed as the dominant source of coupled ocean-atmosphere variability in the North Atlantic Ocean Basin (NAOB). During a positive (negative) phase of the AMM, the Atlantic Intertropical Convergence Zone (ITCZ) is displaced northward (southward), causing drought (excess precipitation) in Northeast Brazil. Warmer (cooler) than normal sea surface temperatures (SSTs) and weaker (stronger) than normal vertical wind shear during positive (negative) phases of the AMM tend to enhance tropical

cyclone development in the NAOB. The AMM is known by NOAA (https://www.aoml.noaa.gov/phod/research/tav/tcv/amm/index.php), to exhibit variability on inter-annual to decadal timescales. Surface air pressure responds to the SST anomalies, becoming higher than normal over the anomalously cold SSTs and lower than normal over anomalously warm SSTs. Anomalous surface winds flow from the cold to the warm hemisphere, strengthening the mean southeasterly trade winds in the South Atlantic and weakening the northeasterly trade winds in the North Atlantic. The surface wind anomalies thus provide a positive feedback onto the initial SST anomalies by forcing changes in wind-induced evaporative cooling of the ocean. The AMM (Table 3) displays 7 IMFs at 2-4, 5-7 and 11-13 months and 2-4, 5-7, 20-22 and 60-70 years. It has moved from positive to negative over the 73 year record (Figure 16), suggesting that the ITCZ has moved southward over the past 7 decades and that there is a tendency for overall enhanced tropical cyclone development in the NAOB.

The Atlantic Multi-decadal Oscillation (AMO), also known as Atlantic Multi-decadal Variability (AMV), is the hypothesized variability of the sea surface temperature (SST) of the NAOB on the timescale of several decades. While there is some support for this mode in models and in historical observations, controversy exists with regard to its amplitude, and whether it has a typical timescale and can be classified as an oscillation. There is also discussion on the attribution of sea surface temperature (SST) change to natural or anthropogenic causes, especially in tropical Atlantic areas important for hurricane development (https://en.wikipedia.org/wiki/Atlantic_multidecadal_oscillation). We show (Table 3) that the AMO displays IMFs centered at 3, 6 and 12 months, and 3, 6, 21 and 65 years, so we have debunked the hypothesis that the AMO only oscillates at a period of several decades, but rather does so at three well-defined monthly periods and four well defined yearly periods, two multiple years, and two multi-decadal; another revelation given the current hypothesis on its internal temporal variability. Its trend is strongly upward, an indication of an overall warming of the NAOB (Table 3, Figure 16).

The Arctic Oscillation (AO), aka the Northern Annular Mode/Northern Hemisphere Annular Mode (NAM), is a weather phenomenon observed at the Arctic pole north of 20 degrees latitude. It is viewed as an important mode of climate variability for the Northern Hemisphere. The southern hemisphere analogue is the Antarctic oscillation or Southern Annular Mode (SAM). The index varies over time and the peer reviewed literature (referenced below in the climate government news) reports that neither the AO or SAM display any particular periodicity, and is characterized by non-seasonal sea-level pressure anomalies of one sign in the Arctic, balanced by anomalies of opposite sign centered at ~ 37–45°N. However as shown in Table 3, we find that is not the case, and we herein debunk that characterization. The AO displays 7 IMFs are centered about 3, 6 and 12 months, and 3, 11, 33 and 65 years, with an overall trend (IMF 8) that began negative and has become increasingly positive over its 73 year record (Figure 16), so the AO is strongly warming. (https://www.climate.gov/news-features/understanding-climate/climate-variability-arctic-oscillation.php).

The North Atlantic Oscillation (NAO) is a weather phenomenon over the North Atlantic Ocean of fluctuations in the difference of atmospheric pressure at sea level (SLP) between the synoptic Icelandic Low Pressure system and the synoptic Azores High Pressure system (https://www.bing.com/search?pc=U523&q=north+atlantic+oscillation&form=U523DF). Through fluctuations in the strength of the Icelandic Low and the Azores High, it is believed to control the strength and direction of westerly winds and location of atmospheric storm tracks across the NAOB. The 201 year record of the NAO is characterized by IMFs of 3, 6, 12 month oscillations and 3, 6, 11, 21, 45, and 110 year oscillations. Over the 201 years of observations the trend is positive, though slightly downwards (Figure 15). The relationship

between the yearly averaged AO and NAO is shown in Figure 13. They trck eh other quite closely.

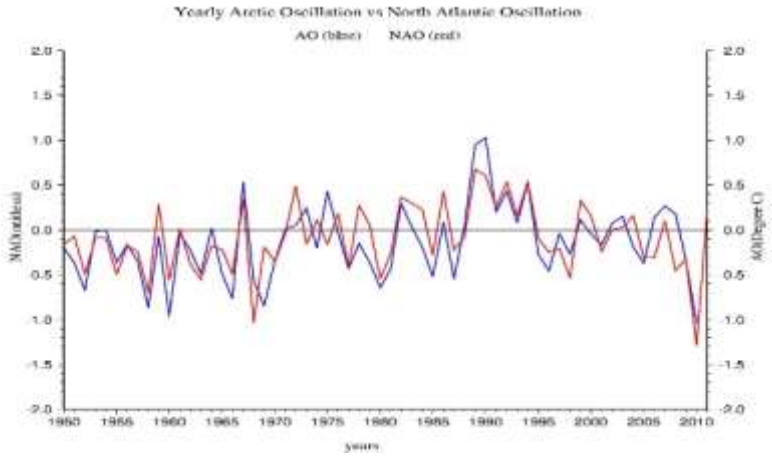

Figure 13. The AO versus the NAO

The El Niño/Southern Oscillation (ENSO) is the interaction between the atmosphere and the ocean and is due to a change in air pressure over the Tropical Pacific Ocean. (https://oceantoday.noaa.gov/elninolanina/welcome.html). Climatologists define these linked phenomena as El Niño-Southern Oscillation that results in what is generally accepted to be a 2-7 year periodic oscillation from warm to neutral to cool waters along the eastern Pacific Ocean Basin (POB) Equatorial zone, a somewhat periodic variation between below-normal and above-normal sea surface temperatures and dry and wet conditions over the course of a few years). While the tropical ocean affects the atmosphere above it, so too does the atmosphere influence the ocean below it. One layer of the eastern POB that is influenced by ENSO is the thermocline. The thermocline marks the transition between the warm upper water and the cold deep water in the POB along the Equator. The upward currents along the equator (or upwelling) are strongest across this transition) temperatures. When the thermocline is closer to the water surface, upwelling of cold, nutrient rich deep-water is transported up from the bottom layers, leading to cooler temperatures at the water surface. The interaction of the atmosphere and ocean is an essential part of El Niño and La Niña events (the term coupled system is often used to describe the mutual interaction between the ocean and atmosphere). During an El Niño (the name for a Spanish boy child), sea level pressure tends to be lower in the eastern Pacific and higher in the western Pacific while the opposite occurs during a La Niña (Spanish for a girl child). This purported see-saw in atmospheric pressure between the eastern and western tropical Pacific is called the Southern Oscillation, often abbreviated as simply the SO. Since El Niño and the Southern Oscillation are related, the two terms are often combined into a single phrase, the El Niño-Southern Oscillation or ENSO. As the phenomenon was historically noted about Christmas, the term ENSO Warm Phase became known to describe El Niño, the "boy child" and the ENSO Cold Phase to describe La Niña, the "girl child". ENSO is touted as the climate factor with the greatest effects globally on weather and climate. The Japanese Meteorological Agency (JMA), the JMA Index, has been a historically constant source of tracking ENSO phases and strengths (https://www.coaps.fsu.edu/jma). As shown in Table 3, the 152 year JMA record of ENSO actually displays ten very distinct IMFs, with periods centered about 3, 6 and 12 months and 3, 6, 11, 21, 65 and 110 years, with a steeply rising overall trend (Figure 13). Thus, we have debunked the hypothesis that ENSO is only a 2-7 year cycle of atmospheric pressure and oceanic surface temperature. Actually, ENSO contains nine modulated modes of oscillation that are occurring simultaneously, and the combinations therein

affects the amplitudes at any particular time, though we note that the strength of ENSO peaks at the periods of 0.5, 1, 3, and 6 years.

The Pacific Decadal Oscillation (PDO) is a pattern of ocean-atmosphere climate variability centered over the mid-latitude POB. The PDO is detected as warm or cool surface waters in the POB, north of 20°N. Over the past century, the amplitude of this climate pattern is reported to have varied irregularly at inter-annual-to-inter-decadal time scales. There is evidence of reversals in the prevailing polarity, i.e., changes in cool surface waters versus warm surface waters within the region of the oscillation occurring around 1925, 1947, and 1977. This climate factor is believed to affect coastal SSTs and continental surface air temperatures from Alaska to California. While the PDO and ENSO are characterized as having similar spatial climate fingerprints, they also have been described as having very different behavior in time (Figure 14) (https://psl.noaa.gov/pdo).

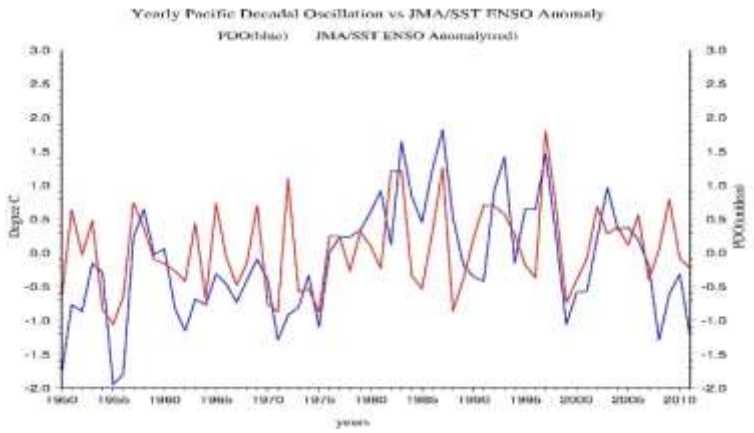

Figure 14. The PDO versus the ENSO

The Florida Current time series is of interest because it sets the upstream condition for the volumetric flux of the Gulf Stream, a Western Boundary Current (WBC). While the time series is relatively short (~ 40 years), there is no other WBC time series on the planet. Many recent articles (Pietrafesa et al., 2022) have investigated two conjectures regarding the Gulf Stream, one that its volumetric flux is in a terminal downward spiral and the other that coastal sea level is affected by it along the U.S. eastern seaboard. That recent study determined that neither conjecture is true. (https://www.aoml.noaa.gov/phod/wbts).

The Global Surface Temperature Anomaly time series consist of three separate planetary time series, one land based (the GLSTA), one ocean surface based (the GOSTA) and the third, the combination of the two (the GSTA). These time series are one of the set of jewels in the crown as they are lengthy in period, are global, and provide global temperature overviews whose trends have been related to Fossil Fuel burning by multiple sources, such as the Intergovernmental Panel on Climate Change (the IPCC) and via a plethora of peer reviewed literature (https://www.ncdc.noaa.gov/cag/global/time-series). However, visual correlation between two or more curves does not prove causality. The only study that proved causality in the econometric Granger Causality sense was that of Pietrafesa, Gallagher, Bao and Gayes (2018). The trend of the GLSTA shows a record length rise of 1.22^{o}C and the GOSTA displays a rise of 0.67^{o}C. The collective GSTA rises 0.88^{o}C. The ocean surface temperature has risen at a much slower rate than the atmosphere over land. This is an excellent example of the power of the EEMD IMF decomposition. The full time series of the GOSTA displays an overall beginning to end of the series increase of 0.75 ^{o}C, the GLSTA shows a rise of 2.91 ^{o}C and the GSTA indicates an overall increase of 1.25 ^{o}C. The three times series are characterized by IMFs at 2-4, 5-7 and 11-13 months and 2-4, 5-7, 10-12, and 20-22 years. Curiously, the ocean surface

temperature time series (the GOSTA) also contains a 60-70 year oscillation, which is reflected in the GSTA. This may be a reflection of the half cycle of the Meridional Oceanic Circulation Conveyor Belt (Pietrafesa et al., 2022), so is absent in the land based temperature series.

Oceanic Heat Content is an important variable to consider for SLV and SLR. These data were collected variously and together by the U.S. Navy following WWII and then beginning in the 1970's by NOAA also. The time series date back to ~ 1950. Arguably, while short in time, they are a jewel in the crown of assessing the causes of SLV and SLR in the Atlantic and the Pacific Ocean Basins (https://www.ncei.noaa.gov/access/global-ocean-heat). If you fill or drain a bathtub, the soap dishes on the sides fill up or empty as well. Coastal sea level is the soap dish analogue. There is a claim (Donovan, 2022) that deep-ocean cooling may have offset global warming until 1990. However our 700m plots of oceanic heating and cooling show no such persistent cooling having occurred after about 1972 (Figure 15). The AOB (left panel) appears to have heated up more rapidly than the POB (right panel). Both the AOB and POB display four IMFs at ~ 2, 3-5, and 7-9 year cycles and overall upward trends. Given the latter, we are dismissing the claim that deep ocean cooling thwarted climate warming.

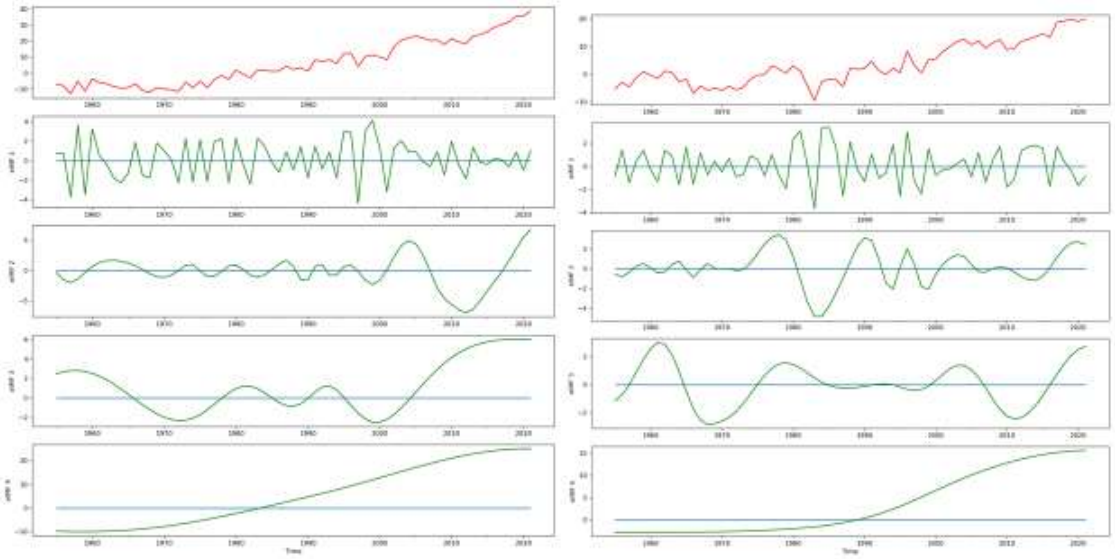

Figure 15. Oceanic Heat Content in the AOB (left panel) and POB (right panel)

The Indian Ocean/West Pacific Anomaly Warm Pool (PACW) extends almost half way around the globe, stretching along the equator south of India, through the waters off Sumatra, Java, Borneo, and New Guinea, and into the central POB. The waters of the Warm Pool (https://earthobservatory.nasa.gov/features/WarmPool) are found by NASA to be warmer than any other open ocean on Earth. These waters are hot enough to drive heat and moisture high into the atmosphere. The slow fluctuations of size and intensity of the warm pool may be linked with the intensity of El Niño's. The PACW trend is strongly upward (Figure 16).

The Oceanic Niño Index (ONI) is NOAA's primary index for tracking the ocean part of ENSO**.** The ONI is a rolling 3-month average temperature anomaly in the surface waters of the east-central tropical Pacific, near the International Dateline. The ONI is characterized by IMFs at 5-7 and 11-13 months, 2-4, 5-7, 10-12, 45-50 year cycles and is downward trending (Figure 16) (https://www.britannica.com/science/Oceanic-Nino-Index).

The Eastern Tropical Pacific (ETP) SST tracks the warm phase of ENSO, wherein the eastern tropical Pacific is characterized by equatorial positive sea surface temperature (SST)

and negative sea level pressure (SLP) anomalies**.** The Western Tropical Pacific is marked by off-equatorial negative SST and positive SLP anomalies. The ETP displays 2-4, 5-7 and 11-13 month IMFs and 2-4, 5-7 and 20-22 year IMFs, and displays an upward trend (Figure 16) (https://www.ospo.noaa.gov/Products/ocean/sst/anomaly).

The Southern Oscillation Index (SOI) (www.bom.gov.au/climate/enso/history/ln-2010-12/SOI-what.shtml*)* is a measure of the intensity or strength of the atmospheric Walker Circulation. It is one of the key atmospheric indices for gauging the strength of El Niño and La Niña events and their potential impacts on the Australian region. The SOI measures the difference in surface air pressure in Tahiti and Darwin Australia. It is characterized by IMFs at 2-4, 5-7 and 11-13 months and 2-4, 5-7, 22-22 and 45-50 years and has a downward trend (Figure 16).

The Antarctic Oscillation Index (AAO) is the difference of zonal mean sea level pressure between 40°S and 65°S. The AOI has the potential for clarifying climate regimes in the southern hemisphere, similar to how the NAO and the NPO has been used in the northern hemisphere (https://www.cpc.ncep.noaa.gov/.../aao/aao_index.html). It displays IMFs at 2-4, 5-7 and 11-13 months and 2-4, 5-7 and 20-22 years. Its trend is downward (Figure 16).

The Atlantic Ocean Basin Heat Content (AHC) and the Pacific Ocean Heat Content (PHC) are the amounts of heat stored in the ocean basins down to 300, 700 and 2000 meters. They display similar IMFs of 2-4, 5-7 and 20-22 years. Their trends are strongly positive and nearly overlay (Figure 16).

Table 2. Climate Factor Details

Climate Factors	**Abbreviation**	**Start Date**	**Start Value**	**End Date**	**End Value**	**Units**
Atlantic Multi-Decadal Oscillation	AMO	01/1856	0.240	12/2021	0.259	C°
Northern Atlantic Oscillation	NAO	01/1821 07/1821	-99.990 -2.624	12/2021 06/2021	-99.990 -1.587	hPA
Global Land + Sea Temperature Anomaly	GLSTA	01/1750	-2.164	05/2021	1.100	C°
Global Sea Temperature Anomaly	GSTA	01/1850	-0.760	12/2021	0.792	C°
Global Ocean Surface Temperature Anomaly	GOSTA	01/1880	0.01	11/2020	0.62	C°
Arctic Oscillation	AO	1/31/1950	-0.06	12/31/2021	0.201	C°
Atlantic Meridional Mode	Atlantic meridional	01/1948	0.660	12/2021	2.690	C°
El Nino Southern Oscillation	ENSO El Nino La Nena	01/1868 03/1868	999 (no value) -2	12/2019 11/2019	999 (no value) 5	Index (temp in C°) Anomaly
Oceanic Heat Content	Northern and Southern Hemispheric Ocean Basins	06/1955 06/1955	-6.925 X 10^{22} -5.402 X 10^{22}	06/2021 06/2021	38.902 X 10^{22} 19.972 X 10^{22}	10^{22} Joules
Eastern Tropical Pacific	ETP	01/1948 01/1950	-99.99 (no value) -2.10	12/20221 01/2022	-99.99 (no value) -1.31	Index (temp in C°) Anomaly

Monthly Sunspot	Sun	01/1749	96.7	12/2021 10/2021	-99.9 (no value) 38.1	Total observed
Pacific Decadal Oscillation	PDO	01/1854	0.11	12/2021	-2.73	Index (sea surface temp in C°) Anomaly
Oceanic Nino Index	ONI	01/1950	-1.53	12/2021	-0.99	Index (temp in C°) Anomaly
Antarctic Oscillation	AAO	01/1979	0.209	12/2020	1.481	Index (temp in C°) Anomaly
Pacific Warm Pool Area Average	PACW	01/1948	-0.622	12/2021 01/2020	-9999 (no value) 0.211	Index (temp in C°) Anomaly
Southern Oscillation Index	SOI	01/1948 01/1950	-99.99 (no value) 2.50	01/2022	0.80	Index (temp in C°) Anomaly
Quasi- Biennial Oscillation	QBO	01/1962				
Florida Current	FC	3/18/1982	30.6	08/08/2021	30.9	Voltage index anomaly

Table 3. Climate Factor IMFs and Amplitudes

Climate Factor	IMF's Length of Series	2-4 mnth	5-7 mnth ---	11-13 mnth	2-4 yrs	5-7 yrs	10-12 yrs	20-22 yrs	30-33 yrs	45-50 yrs	60-70 yrs	110 yrs	150, 540 yrs
Solar Sunspot	273 5-408 events	50	50	40	40	---	120	40	---	40	---	20	15, 4
ENSO	152	2	5	10	10	6	3	2	---	---	2	1.5	---
PDO	115	1	1	1	1	1	1	0.5	---	---	0.2	0.1	
AMO	167	0.2	0.2	0.2	0.2	0.2		0.1	---	---	0.2	---	0.1
NAO	201	4	2	2	2	1	0.5	0.4	---	0.2	---	0.1	---
GOSTA	140	0.1	0.1	0.2	0.1	---	0.1	0.1	---	---	0.2	---	
GLSTA	270	4	3	2	0.5	0.3	0.25	0.1	---	---	---	---	---
GSTA	170	0.2	0.2	0.2	0.2	0.2	0.1	0.1	---	---	0.2		---
AO	71	2	1	1	1	---	0.2	---	0.1	---	0.1	---	
AMM	73	3	4	3	3	2	---	1	---	---	1		
AAO	42	1	1	1	0.7	0.2	---	0.1	---	---			
ONI	71	---	1	1	1	1	0.4	---	---	0.4	---		
PWPAA	73	0.2	0.2	0.2	0.2	0.1	---	0.05	---	---			
SOI	73	2	2	2	2	2	---	0.5	---	0.5			
AHC	65	---	---	---	4	5	---	6	---	---			
PHC	65	---	---	---	4	4	---	3	---	---			
ETP	73	0.5	0.5	1.0	1.0/ 1.0	1.0	---	0.3					
QBO	62	0.5	0.5	1.0	20	1.0	---	0.5	---	0.2			

FC/GS	38	5.0	4.0	3.0	1.5	0.6	1.0						
Fossil Fuel	265				4-6 yrs 200 MMT		8-10 yrs 200 MMT						---

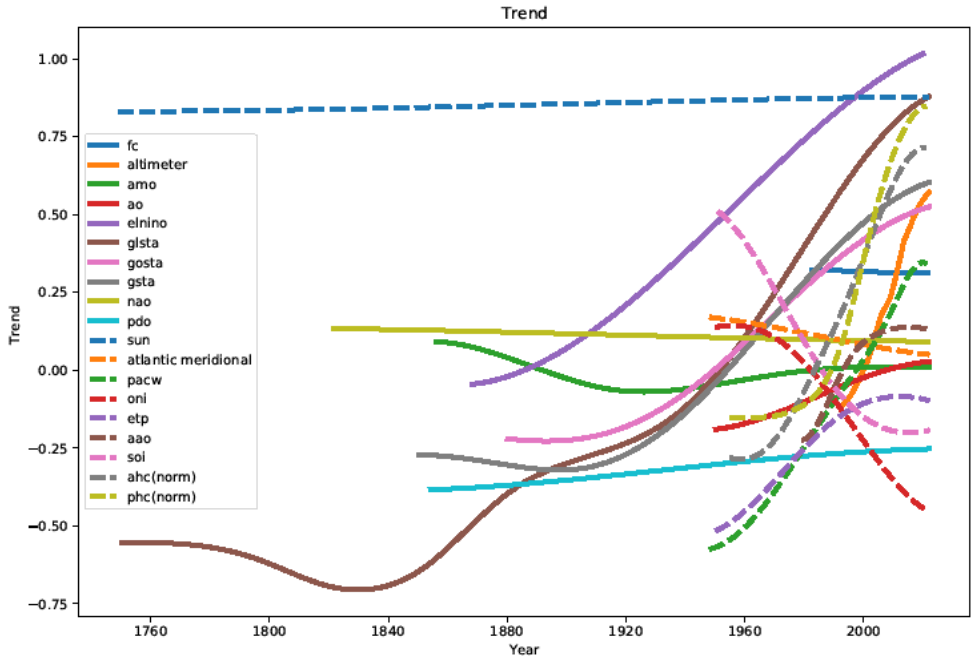

Figure 16. Trends of Selected Climate Factors

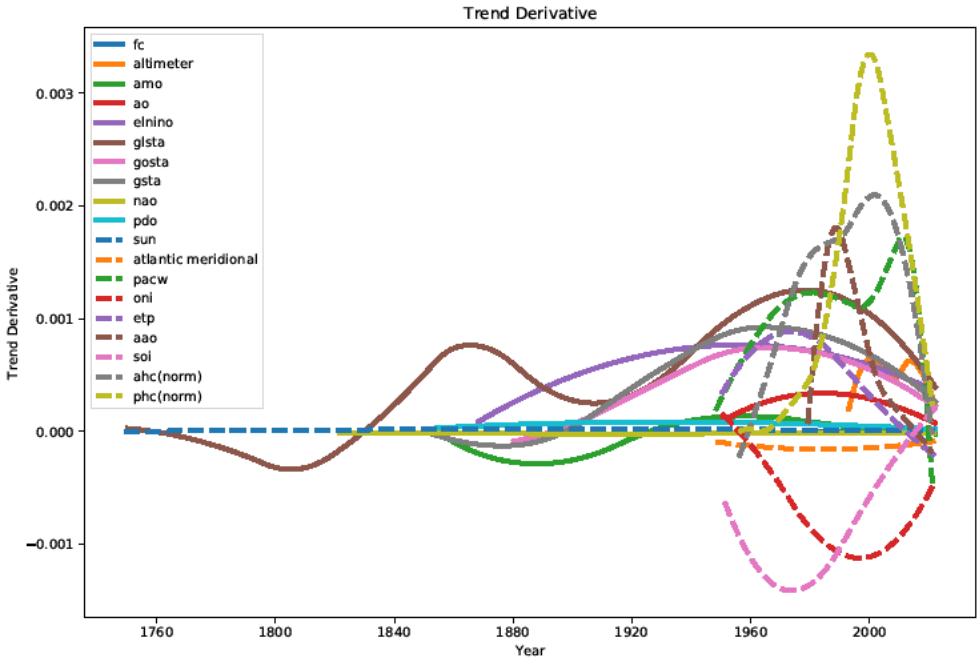

Figure 17. Rates of change (1st derivatives) of selected Climate Factors

SEA LEVEL VARIABILITY AND CLIMATE FACTORS

As can be seen in Tables 2 and 4, the IMFs of SL and the selected Climate Factors are in sync at seasonal to annual to inter-annual, to multi-year to decadal for all stations, to inter-decadal to multi-decadal time scales for 5 of the eleven stations, and out to four decades for

Auckland, Sydney, Honolulu and San Francisco. A mode by mode cross-correlation was not done as it is beyond the scope of this study. However, it may be possible to conduct such an analysis in the future. The individual IMFs of the SL time series could be cross-correlated with the IMFs of the Climate Factors. That said, some revealing relationships can be created between individual stations and selected climate factors, by way of example.

ENSO is a well-known global climate factor. However, the conventional notion of ENSO is that it is an around 5-year quasi-periodic phenomenon. But Table 4 reveals otherwise. ENSO is far more complicated in that it is characterized by many more intrinsic modes of variability. In fact it has an ~ 110 year mode with amplitude range of +/- 0.15^{o}C, an ~ 60 year mode of +/- 0.2 ^{o}C range, a 30-35 year mode of 0.3^{o}C range, a 10-12 year mode of +/- 0.3^{o}C, a 5 to 7 year mode of +/- 0.8^{o}C range, a 2-4 year mode with range +/- 1.0^{o}C, an annual mode of +/- 0.9^{o}C range and a 0.3-0.8 year mode of +/- 0.8^{o}C range. This is quite an array of modes, all superimposed, all running at the same time, and all distinct. The concept of "cold" and "warm" 3-4-year ENSO phases just does not do this climate factor justice. There have been periods in the past, such as 1878, 1893, 1917, 1940, 1955, 1958, 1983, 1988, 1998, and others, when many of the ENSO IMF modes were in the same phase and super warm and super cold phases of ENSO occurred. During these warm (cold) episodes, San Francisco, San Diego, Seattle and Honolulu sea levels rose (fell) dramatically apparently in a steric response. So North Pacific Ocean eastern boundary coastal sea levels appear to be well correlated with ENSO phases. A straightforward match of annually averaged ENSO vs San Francisco sea level is shown in Figure 18. The comparison shows that there is a great deal of similarity in the two time series. This is true, to varying degree, for other Pacific Ocean Basin coast water levels as well. So ENSO and San Francisco sea levels are generally in phase, and the longer period adjustment of warm to cool and rises and falls, respectively, are generally in agreement. The peaks and valleys of the MSL of San Francisco and ENSO warm and cold phases are totally in sync and departures in the amplitudes can be attributed to the lower and higher frequency IMF's of either time series. The relationship shows remarkable agreement.

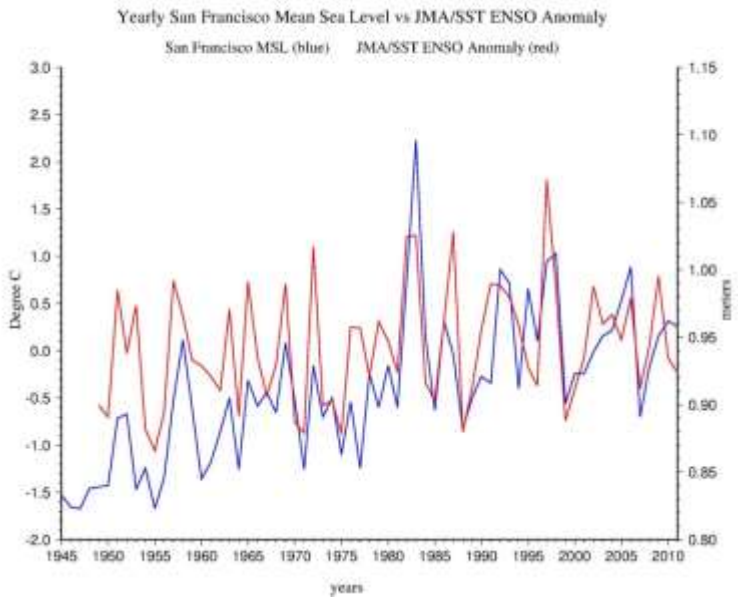

Figure 18. Annually averaged time series of the ENSO Index and San Francisco CA USA Sea Level

The conclusion here is that SLV IMFs and Climate Factor IMFs are in sync and sea level responds to what is happening on higher to lower frequency changes in what the atmosphere and ocean are doing over very large spatial and temporal scales.

FOSSIL FUEL BURNING TIME SERIES

In Figure 19, we present the Fossil Fuel Burning data time series extending back to the mid-18th Century. These data are meticulously kept. The CE time series beginning in 1751 was provided to us via (http://cdiac.ornl.gov/trends/emis/tre_glob.html). Global CO_2 Emissions from Fossil-Fuel Burning, Cement Manufacture, and Gas Flaring: 1751-2013. Confirming sources also include: 1) T. Boden and R. Andres, The Carbon Dioxide Information Analysis Center, Oak Ridge National Laboratory, Oak Ridge, Tennessee 37831-6290, USA; and 2) G. Marland, The Research Institute for Environment, Energy and Economics, Appalachian State University, Boone, North Carolina 28608-2131, USA. The time series now extends from 1751 through 2018. It began at 3 Million Metric Tons (MMT) in 1751 and by 2018 had risen to 10,083 MMT. The time series contains 3 IMFs, IMF 1 at 3-5 years and 200 MMT in amplitude, IMF 2 at 8-10 years and 200 MMY in amplitude and IMF 3, the trend. The curve was relatively flat for 120 years, then rose slowly until 1950, and exploded upward thereafter to the present.

In Figure 20, the Global Surface Temperature Anomaly (GSTA) plot, from 1850 to 2020, displays 8 EEMD IMFs and IMF 9, which is an overall trend, similar to the Fossil Fuel Burning Trend. While this visual correlation is strong, it does not prove attribution. However, Pietrafesa et al. (2019) invoked Granger Causality (Granger, 1966) to prove attribution of GSTA's and FFB. This was a major finding. As FFB is global, we will now test the global sea surface satellite altimeter time series trend against FFB, and determine if there is an attributive relationship.

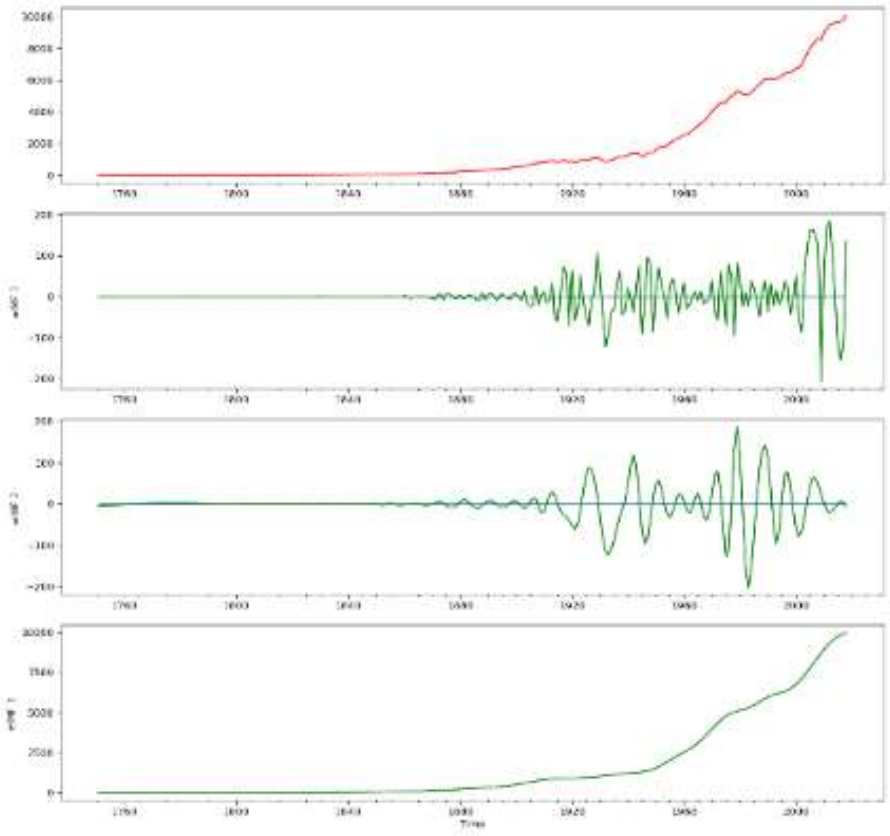

Figure 19. Fossil Fuel Burning Curve displaying 3 EEMD IMFs of Fossil Fuel Burning since the early 1700's to 2022

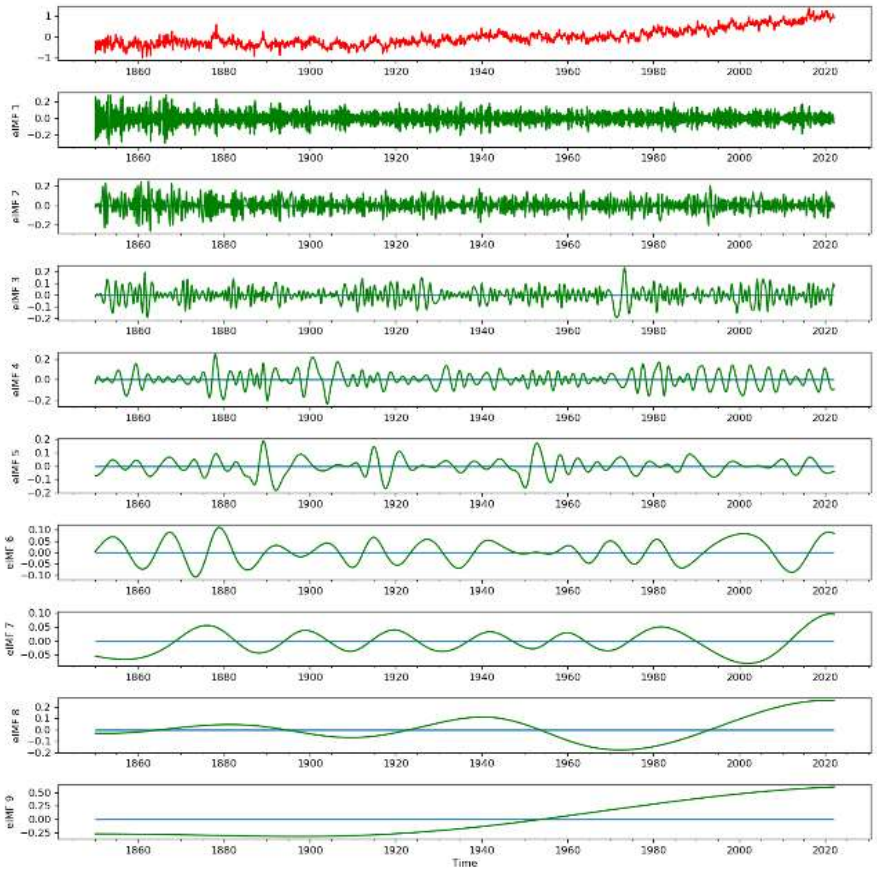

Figure 20. The Global Surface Temperature Anomaly Time Series, 8 time varying IMFs and its overall trend (Pietrafesa et al., 2022)

ATTRIBUTION BETWEEN FFB AND ALT

Granger Causality (Granger, 1966) analysis is used to find the dependency of one time series on another one, generally employed in the fields of Econometrics and Neuroscience. If the prediction of one time series can be improved using the past knowledge of the second time series, then the second one is said to have a causal influence on the first one. Below we attempt to relate global altimeter observations of the sea surface with fossil fuel burning.

The range of the altimeter data, which began in 1992 and the extent of the fossil fuel time series which ended in 2018 were the limiting factors. To calculate the Granger Causality we test the null and alternative hypothesis, where H_0 represents the time series x, the altimeter data (ALT), which is found to not "Granger Cause" the time series H_A which represents the time series y for fossil fuel burning (FFB). Next we look to the FFB to cause rises in the ALT.

$$x_t = \sum_{j=1}^{p} A_{11}\, x(t-j) + \sum_{j=1}^{p} A_{12}\, y(t-j) + e_1 \quad (2)$$

$$y_t = \sum_{j=1}^{p} A_{21}\, x(t-j) + \sum_{j=1}^{p} A_{21}\, y(t-j) + e_2 \quad (3)$$

In the Equations 2 and 3, p represents the maximum number of lagged observations included in the model, A represents the matrix containing the coefficients of the model, and e_1, e_2 is the residuals for each time series at time t. The time series y_t (herein FFB) is said to be Granger Causing x_t (ALT), if the variance of the residuals are reduced after the inclusion of y_t terms in the Equation 3 or vice versa. Also, the coefficients within the matrix A_{12} needs to be different from zero. This is tested by calculating the F-test score. If the F-test score is greater than 2.5 and probability (p-value) is less than 0.05, we can reject the Null hypothesis described above and say that one time series y_t (FFB) Granger Causes another time series x_t (ALT).

Herein, we have used the *grangercausalitytests* python library for getting the F-test score and p-value for these two time series.

As it takes one year for the planet to change its surface temperature (GSTA) after the increase in Fossil fuel burning, we set up this same lag of 1 year while establishing a causality between Fossil Fuel burning and the rise of sea level, considering it might take 1 year to reflect the change in sea level due to fossil fuel burning. To make the causality robust, this time we normalized the data points. We achieved F-test score of 2.55 and chi-2 based p-value 0.0117. So, we can reject the null hypothesis and say that the rise in FFB is Granger Causing the rise in the ALT time series. Finally, we have used a regression model to predict the sea level rise value from the past values of time series of Fossil fuel burning and compared the prediction with actual sea level rise value with 95% above and below confidence interval.

Similarly, we checked the p-value and F-test while setting up the lag of 2 and 3 years as well. From Table 5. We can see that we achieved the highest score in the F-test when we shifted the time series of Sea Level rise with lag of 3 years. So, it can be assumed that FFB is affecting and causing the sea level rise after a 3 year gap. The length of our dataset is somewhat compact to consider the 3 year lagged values but we can still consider it for our prediction. However, the lag year of 2 could not pass the threshold of Granger causality and so we will not consider prediction using lag 2.

Table 5. Granger Causality Lags between FFB and ALT and Parameters

Lag in Years	F-test Score	p-value
1	2.5508	0.00117
2	2.0844	0.12270
3	3.6879	0.03950

We have used the year of 2017 and 2018 for predicting the ALT, sea level rise values with the past values of FFB, fossil fuel burning values. From Figure 21, we see the actual and predicted values are very close (Actual is 0.814471865 and predicted is 1.003710). For the year of 2018 the actual value of sea level rise is -0.062427213 but the predicted value is 1.021130. Therefore, from analyzing the Figure 21 we establish that Fossil Fuel burning time series is Granger Causing the Sea level rise time series and past values of FFB time series can be used to predict future sea level rise values. We have also plotted the prediction values for year lag of 3, as shown in Figure 22. For the year of 2017 and 2018, the predicted values are 0.94804134 and 0.96541817 which are much closer to the actual values. So, we can say that causality is established in a better way when the sea level rise time series is shifted 3 years to see the effect of FFB rather than a 1 or 2 year lag.

Although the dataset is relatively short (27 years of ALT values), we performed regression analysis to check the accuracy for prediction model. The testing accuracy was 94.68% which indicates the robustness of the model's prediction of sea level rise with the Fossil fuel burning past values.

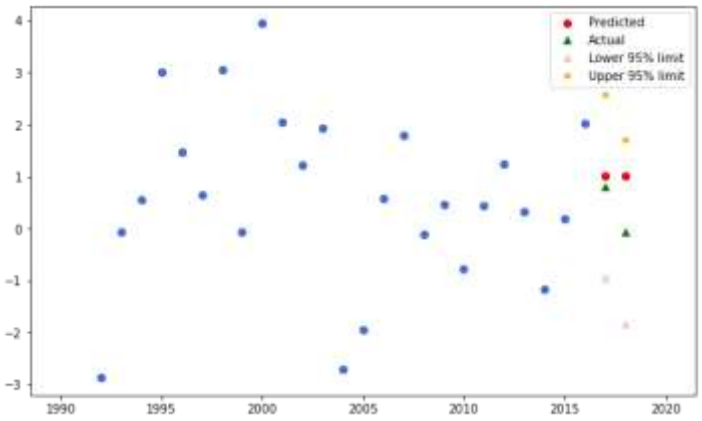

Figure 21. Fossil Fuel Burning vs. Sea Level rise Causality Analysis (Lag of 1- year)

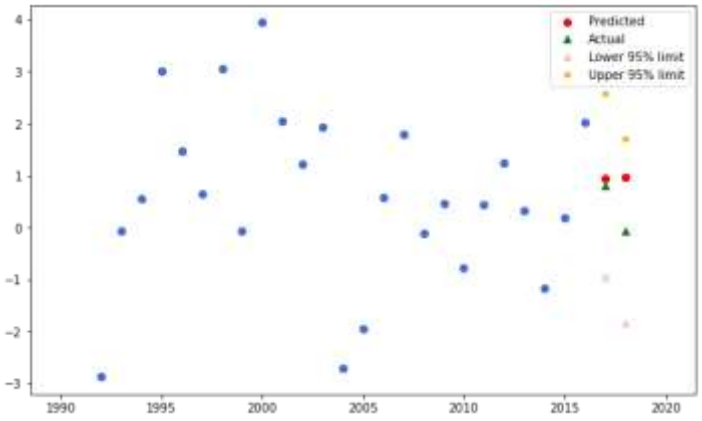

Figure 22. Fossil Fuel Burning vs. Sea Level rise Causality Analysis (Lag of 3 years)

SUMMARY AND CONCLUSIONS

To properly understand the facts of sea level variability and rise globally, we have harvested and evaluated 11 open ocean coastal sea level stations that displayed relatively long, continuous time series. Additionally we harvested the continuous time series of multiple satellite altimeter data sets, which are only 30 years long. Our goals were to seek to reveal correlative relationships between SLV and SLR and Climate Factors and moreover, to determine if there was an attributive relationship between FFB and SLR as measured by ALT. This is important in that at least half of the world's population lives at or near the coast, and is at risk from SLR and atmospheric storms. The ability to numerically model incoming storm surge and inundation is strongly dependent on the stand of coastal sea level, to set the initial boundary conditions. We have revealed that FFB does indeed effect SLR with a three-year phase lag. Operational forecasting of surge and inundation and on increasing numbers of Blue Sky floods around planet Earth will continue to increase with increasing FFB.

While Pietrafesa et al. (2019) demonstrated that there was a 1-year lag between Fossil Fuel Burning and Global Surface Temperature changes over land globally and at the surface of the global ocean, there is a 3 - year lag between the adjustments of sea level globally. This may be due to a water column steric adjustment time scale and has not been previously reported in the literature. Thus, it may take 2 years for Heat to penetrate from the Surface of the Ocean down to depths of 300 and/or 700 and/or 2000m in the Ocean Basins.

We conclude that the rise of sea level globally, via fossil fuel burning induced anthropogenic warming, is changing the level of the ocean in all of the World's ocean basins. Thus, coastal sea level will continue to rise at the mouths of the rivers, harbors and estuaries globally. So modeling of future surge and inundation must take into account the continued

burning of fossil fuels, possibly at an increasing rate. Moreover, these coastal systems will be put into ever increasing storage modes as the global oceans blocks discharges of the land based water systems. Compound flooding will become more complex and saltwater intrusions into inshore systems, including the groundwater tables will increase, as salt water will replace fresh water, pushing the fresh water upward leading to more saturated ground in the coastal areas of the world.

Site specific coastal sea level and global ocean altimeter time series all display frequency and amplitude modulated 3 monthly seasonal, half-year, annual, inter-annual, multi-year, decadal, inter-decadal and multi-decadal variability. Remarkably, the same intrinsic frequency and amplitude modes of variability are revealed in the decompositions of the climate factor data. So, atmospheric and oceanic temperatures and atmospheric pressures are beating together, all at the same modulated frequencies, and sea levels globally reflect those beats with internal modes of variability that are consistent with each other and with the climate factors. The amplitudes of the climate factor intrinsic modes of variability change through recorded time, and so do the sea level internal modes of variability. Across the ranges of sea level variability, the amplitudes of higher and lower frequency modes are generally of similar values on a station by coastal station basis and are reflected in the altimeter data as well.

We demonstrated that coastal sea level, which reflects the astronomical tides globally, is also dominated by the along coast component of coastal winds from hours to days. Moreover the same relationship holds true for annual averages of along coast winds and set up and set down of coastal sea level. Moreover, climate factors, such as ENSO can dominate coastal sea level, such as U.S. Pacific coast rises (drops) in sea level during warm (cool) phases of ENSO, and is an area ripe for further research globally. We also uncovered relationships between climate factors, such as the AO and NAO that have not been previously reported in the literature but are clearly relevant to coastal sea level variability. These relationships will be further pursued in Part II of this study.

The overall trends of sea level globally are all increasing, though at different rates. This is due in part to where the stations are located around the planet. In some cases, groundwater extraction has exacerbated the trend of sea level rise as sinking land suggests a relative rise in sea level, and we could not account for those occurrences. In other cases, such as harbor locations, increases or decreases in river discharge could be reflected in rising or more slowly rising water levels. We could not correct for those occurrences either, as we did not study either precipitation changes or river discharge changes over time. However, we did investigate the possible relationships between fossil fuel burning and the trends in sea level over time, in a search for attribution. Rather than investigating relationships of FFB and site specific trends in SLR, we investigated the possible relationship between FFB and the global rise in sea levels measured by satellite altimeters or ALT.

This study is intended to lay the groundwork for a study of the cross-correlation relationships between Sea Level Variability and Rise with the Climate Factors followed by a study of potential causality and attribution between the trends in Sea Level Rise at the 11 individual coastal sea level stations and fossil fuel burning, and projections into the future for each station, given the projections of the IPCC.

ACKNOWLEDGEMENTS

The Authors acknowledge support for this study from: the NOAA National Weather Service's Cooperative Institute for Research to Operations in Hydrology (CIROH) through the NOAA Cooperative Agreement with the University of Alabama (NA22NWS4320003); and the Computational and Information Systems Laboratory. 2019. Cheyenne: HPE/SGI ICE XA System (Climate Simulation Laboratory). Boulder, CO: National Center for Atmospheric Research. doi:10.5065/D6RX99HX.

REFERENCES

Battisti, D. S., & Clarke, A. J. (1982). A simple method for estimating barotropic tidal currents on continental margins with specific application to the M 2 tide off the Atlantic and Pacific coasts of the United States. *Journal of Physical Oceanography*, *12*(1), 8-16.

Bromirski, P. D., Cayan, D. R., Graham, N., Tyree, M., & Flick, R. E. (2012). *Coastal Flooding Potential Projections: 2000-2100.* California Energy Commission. CEC-500-2012-011.

Cazenave, A., & Nerem, R. S. (2004). Present-day sea level change: Observations and causes. *Reviews of Geophysics*, *42*(3), RG3001.

Chao, S. Y. & Pietrafesa, L. J. (1980). The sub-tidal response of sea level to atmospheric forcing in the Carolina Capes. *Journal of Physical Oceanography, 10*(8), 1246-1255.

Chatfield, C. (1975). *The Analysis of time series: Theory and Practice*. John Wiley & Sons.

Church, J. A. (2001). How fast are sea levels rising? *Science*, *294*(5543), 802-803.

Church, J.A., & White, N.J. (2006). A 20th century acceleration in global sea-level rise. *Geophysical Research Letters, 33*, L01602-L01604.

Cione, J. J., Black, P. G. & Houston, S. H. (1999). Surface observations in the hurricane environment. *Mon. Weather Rev., 128*, 1550–1561.

Clark, A. J. (1988). Inertial wind path and sea surface temperature patterns near the Gulf of Tehuantepec and Gulf of Papagayo. *Journal of Geophysical Research, 93*(12), 15491-15501

Coastal Resources Management Council. (1999). RI Salt Pond Region: Special Area Management Plan. CRMC, 150 p.

Coastal Resources Management Council. (2007). The State of Rhode Island Coastal Resources Management Program: As Amended. CRMC, 222 pp.

Donnelly, J.P., Cleary, P., Newby, P., & Ettinger, R. (2004). Coupling instrumental and geologic records of sea-level change: Evidence from southern New England of an increase in the rate of sea-level rise in the late 19th century. *Geophysical Research Letters, 31*, L05203-L05206.

Donovan, R. (2022). Deep-ocean cooling may have offset global warming until 1990. *EOS, 103*(1), 17.

Douglas, B.C. (1991). Global sea level rise. *Journal of Geophysical Research, 96*(C4), 6981-6992.

Douglas, B.C. (1997). Global sea rise: A redetermination. *Surveys in Geophysics*, *18*(2/3), 279-292.

Ezer, T. (2013). Sea level rise, spatially uneven and temporally unsteady: Why the U.S. East Coast, the globaltide gauge record, and the global altimeter data show different trends. *Geophys. Res. Lett., 40,* 5439–5444. https://doi.org/10.1002/2013GL057952

Federal Emergency Management Agency. (1991). Federal Insurance Administration: Projected Impact of Relative Sea Level Rise on the National Flood Insurance Program: FEMA.

Gabor, D. (1946). Theory of communication. Part 1: The analysis of information. *Journal of the Institution of Electrical Engineers-part III: radio and communication engineering, 93*(26), 429-441. https://doi.org/10.1049/ji-3-2.1946.007

Geisler, C., & Currens, B. (2017). Impediments to inland resettlement under conditions of accelerated sea level rise. *Land Use Policy, 66*, 322-330.

Gornitz, V., & Lebedeff, S. (1987). Global sea-level changes during the past century. In D. Nummendal, O.H. Pilkey & J.D. Howard (Eds.), *Sea-level fluctuations and coastal evolution* (Vol. Special Publication No. 41, pp. 3-16). Society of Economic Paleontologists and Mineralogists.

Granger, C.W.J. (1966). The typical shape of an econometric variable. *Econometrica, 34*, 150-161.

Gregory, J. M., Huybrechts, P., & Raper, S. C. (2004). Threatened loss of the Greenland ice-sheet. *Nature*, *428*(6983), 616.

Houston, J.R. & Dean, R.G. (2011). Sea level Acceleration Based on U.S. Tide Gauges and Extensions of Previous Global-Gauge Analyses. *Journal of Coastal Research, 27*(3), 409–417.

Huang, N. E. & Wu, Z. (2008). A review on Hilbert-Huang Transform: the method and applications on geophysical studies. *Rev. Geophys., 46,* RG2006. https://doi.org/doi:10.1029/2007RG000228

Huang, N. E., Shen, Z., & Long, S. R. (1999). A new view of nonlinear water waves: the Hilbert spectrum. *Annual Review of Fluid Mechanics*, *31*(1), 417-457.

Huang, N. E., Wu, M. L. C., Long, S. R., Shen, S. S., Qu, W., Gloersen, P., & Fan, K. L. (2003). A confidence limit for the empirical mode decomposition and Hilbert spectral analysis. *Proceedings of the Royal Society of London. Series A: Mathematical, Physical and Engineering Sciences*, *459*(2037), 2317-2345.

IPCC Climate Change. (2001). The Scientific Basis. Contribution of Working Group 1 to the Third Assessment Report of the Intergovernmental Panel on Climate Change. Cambridge, UK and New York, NY: Cambridge University Press.

IPCC Climate Change. (2007a). The Physical Science Basis. Summary for Policymakers. Contribution of Working Group I to the Fourth Assessment Report of the Intergovernmental Panel on Climate Change. Geneva, Switzerland: UNEP.

IPCC Climate Change. (2007b). Impacts, Adaptation, and Vulnerability. Summary For Policymakers. Contribution of Working Group II to the Fourth Assessment Report of the Intergovernmental Panel on Climate Change. Geneva, Switzerland: UNEP.

James, G., Alchian, A. A., & James, R. C. (1976). *Mathematics dictionary*. Van Nostrand Reinhold Company. ISBN 10: 0442240910 ISBN 13: 9780442240912.

Levitus, S., Antonov, J. I., Boyer, T. P., Locarnini, R. A., Garcia, H. E., & Mishonov, A. V. (2009). Global ocean heat content 1955–2008 in light of recently revealed instrumentation problems. *Geophysical Research Letters*, *36*(7).

Liu, H. (1998). The empirical mode decomposition and the Hilbert spectrum for nonlinear and non-stationary time series analysis. *Proc. Roy. Soc. Lond., 454A*, 903-993.

Mantua, N. J., Hare, S. R., Zhang, Y., Wallace, J. M., & Francis, R. C. (1997). A Pacific interdecadal climate oscillation with impacts on salmon production. *Bulletin of the American Meteorological Society*, *78*(6), 1069-1079.

Mcgranahan, G., Balk, D., & Anderson, B. (2007). The rising tide: Assessing the risks of climate change and human settlements in low elevation coastal zones. *Environment and Urbanization*, *19*(1).

Mitchell, M., Hershner, C., Herman, J., Schatt, D. E., & Eggington, E. (2013). *Recurrent flooding study for Tidewater Virginia.* Virginia Senate Document No. 3.

Mitchell, M., Stiles Jr, W. A., & Hartley, T. W. (2014). Sea level rise: a relentless reality hat Virginia must continue to plan carefully for. *The Virginia News Letter*, *90*(6).

Moran, J. M. (2011). *Ocean Studies: Introduction to Oceanography* (3rd ed.). American Meteorological Society.

NOAA. (2005). Mean Sea Level Trend: 8452660 Newport, Rhode Island. http://tidesandcurrents.noaa.gov/sltrends/sltrends_station.shtml?stnid=8452660%20Newport,%20RI

Overpeck, J.T., Otto-Bliesner, B.L., Miller, G.H., Muhs, D.R., Alley, R.B., & Kiehl, J.T. (2006). Paleoclimate evidence for future ice-sheet instability and rapid sea-level rise. *Science*, *311*, 1747-1750.

Pietrafesa, L. J., Bao, S., Yan, T., Slattery, M., & Gayes, P. T. (2015). On Sea Level Variability and Trends in United States Coastal Waters and Relationships with Climate Factors. *Advances in Adaptive Data Analysis*, *7*(01n02), 1550005.

Pietrafesa, L. J., Dickey, D. A., Gayes, P. T., Yan, T., Epps, J. M., Hagan, M., Bao, S., & Peng, M. (2013). On atmospheric-oceanic-land temperature variability and trends. *International Journal of Geosciences*, *4*(02), 417-443.

Pietrafesa, L.J. & Dickey, D. (2000). *The surge and flood due to Hurricanes Floyd and Dennis.* East Carolina University Press.

Pietrafesa, L.J. & Janowitz, G. S. (1980). On the dynamics of the Gulf Stream front in the Carolina Capes. In *Proceedings of the 2nd International Symposium on Stratified Flows*, pp. 184-187. Trondheim, Norway, 24-27 June, 1980. Tapin Publishing Co.

Pietrafesa, L.J. (2000). *On Sea Level Variability*. Documented Presentation at the Plenary Session of the Board of Oceans, Atmosphere and Climate at the National Association of State Universities and Land Grant Colleges Conference, in Washington DC, Nov. 2000.

Pietrafesa, L.J., Blanton, J.O., Wang, J.D., Kourafalou, V., Lee, T.N. & Bush, K.A. (1980). The tidal regime in the South Atlantic Bight. In L.P. Atkinson, D.W. Menzel, & K. A. Bush (Eds.), *Oceanography of the Southeastern U.S. Continental Shelf, Coastal and Estuarine Sciences* (Vol. 2, pp. 63-76). AGU, Washington, D.C.

Pietrafesa, L.J., Janowitz, G. S. & Wittman, P. A. (1985). Physical oceanographic processes in the Carolina Capes. In L.P. Atkinson, D.W. Menzel, & K. A. Bush (Eds.), *Oceanography of Southeastern U.S. Continental Shelf, Coastal and Estuarine Sciences* (Vol. 2, pp. 23-32). AGU, Washington, D.C.

Pietrafesa, L.J., Janowitz, G.S., Chao, T.-Y., Weisberg, R.H., Askari, F., & Noble, E. (1986). *The physical oceanography of the Pamlico Sound*. UNC Sea Grant Publication UNC-WP-86-5, Raleigh, N.C.

Rahmstorf, S. (2007). A semi-empirical approach to projecting future sea-level rise. *Science, 315*, 368-370.

Rahmstorf, S., Cazenave, A., Church, J.A., Hansen, J.E., Keeling, R.F., Parker, D.E., & Somerville, R.C.J. (2007). Recent climate observations compared to projections. *Science, 316*(5825), 709.

Stern, N. (2007). *The economics of climate change: The Stern review*. Cambridge, UK: Cambridge University Press.

Titus, J.G., & Narayanan, V. (1995). *The probability of sea level rise* (No. EPA 230-R95-008.). Washington, D.C.: U.S. Environmental Protection Agency.

Titus, J.G., & Richman, C. (2001). Maps of lands vulnerable to sea level rise: modeled elevations along the US Atlantic and Gulf coasts. *Climate Research, 18*(3), 205-228.

U.S. Global Change Program National Climate Change Report 2021: https://www.climatecentral.org/gallery/graphics/sea-level-rise-and-population-impact

Union of Concerned Scientists. (2006). Climate change in the U.S. Northeast: A report of the Northeast climate impacts assessment. Cambridge, MA: UCS Publications.

Wu, Z., & Huang, N. E. (2004). A study of the characteristics of white noise using the empirical mode decomposition method. *Proceedings of the Royal Society of London. Series A: Mathematical, Physical and Engineering Sciences*, *460*(2046), 1597-1611.

Wu, Z., & Huang, N. E. (2009). Ensemble empirical mode decomposition: a noise-assisted data analysis method. *Advances in Adaptive Data Analysis, 1*(1), 1-41.

Wu, Z., Huang, N. E., & Chen, X. (2009). The multi-dimensional ensemble empirical mode decomposition method. *Advances in Adaptive Data Analysis*, *1*(03), 339-372.

Wu, Z., Huang, N. E., Long, S. R., & Peng, C. K. (2007). On the trend, detrending, and variability of nonlinear and nonstationary time series. *Proceedings of the National Academy of Sciences, 104*(38), 14889-14894.